NTNU
Norwegian University of
Science and Technology

Modeling, analysis and joystick control of the "AMV Oil Spill Fighter"

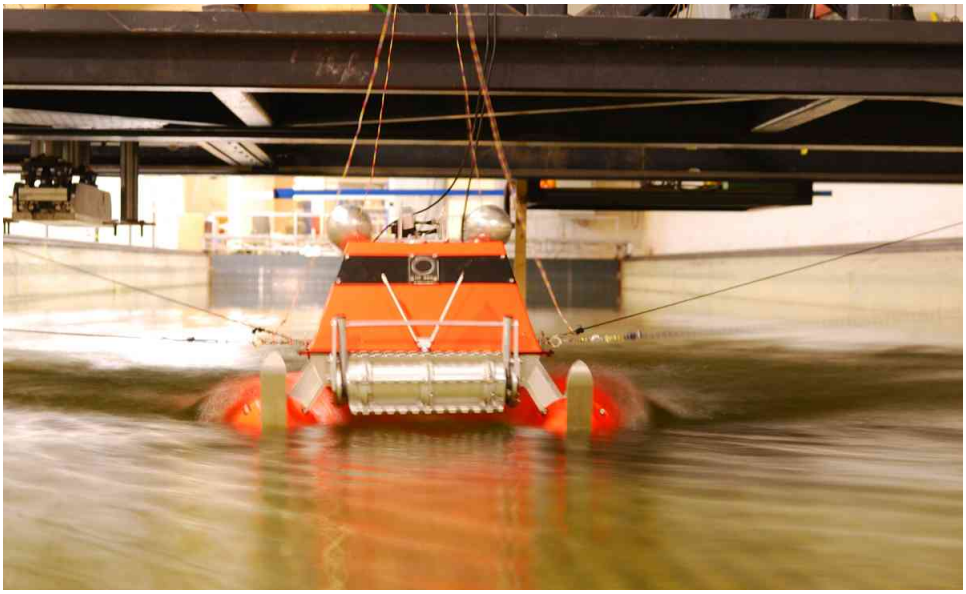

Author:
Lars Martin Fure Nilsen

June 21, 2011

NTNU Trondheim
Norwegian University of Science and Technology
Department of Marine Technology

MASTER THESIS IN MARINE CYBERNETICS

Name of the candidate: Stud. techn. Lars Martin Fure Nilsen

Field of study: Marine control engineering

Thesis title (Norwegian): Modellering, analyse, og joystick-basert fjernstyring av fartøyet "AMV Oil Spill Fighter"

Thesis title (English): Modeling, analysis, and joystick control of the "AMV Oil Spill Fighter"

Background
Current oil protection equipment does not operate well in the transition zone between land and water for several reasons:

- Reefs and shallow water makes it too risky for normal human operated vessels to operate, and thus illegal according to the Norwegian Health, Safety, and Environment (HSE) regulations.
- The amphibious equipment used today is depending on easy access to the polluted area. This is rarely the case.
- No effective method of transport between land and sea exists.

For the "Arctic Multipurpose Vehicle Oil Spill Fighter" (AMV OSF) to aid in solving these problems, the main issue is to remove the danger to the human operator, thus satisfying the HSE regulations. This can be done by a remote control system.

The task of this thesis is to derive and identify a mathematical model of the AMV OSF, that is, a model of the motion dynamics and the thrust devices, and using this model to simulate and analyse the properties and behavior of the vessel. Finally, based on the thrust model and motion dynamics, the task is to develop and test a remote joystick control for the vessel.

Work description

1. Develop detailed mathematical models of the AMV OSF. The models should include vehicle dynamics and propulsion by the Archimedes screws for motion on land and in water for calm sea.
2. Perform system identification of the mathematical models by experimental testing in MC Lab. Validate the mathematical models against the experimental behavior of the vehicle.
3. Discuss the dynamic properties of the vehicle w.r.t. speed, bollard pull, maneuverability, and efficiency of the Archimedes screws.
4. Develop a thrust allocation algorithm, mapping desired motions on land and desired generalized forces (within allowed configuration space) in water to thruster speeds.
5. Develop a joystick command function, including necessary HMI functions, for motion on land and in water.

Guidelines
The scope of work may prove to be larger than initially anticipated. By the approval from the supervisor, described topics may be deleted or reduced in extent without consequences with regard to grading.

The candidate shall present his personal contribution to the resolution of problems within the scope of work. Theories and conclusions should be based on mathematical derivations and logic reasoning identifying the various steps in the deduction.

The report shall be organized in a rational manner to give a clear exposition of results, assessments, and conclusions. The text should be brief and to the point, with a clear language. The report shall be written in

English (preferably US) and contain the following elements: Abstract, acknowledgements, table of contents, main body, conclusions with recommendations for further work, list of symbols and acronyms, references and (optional) appendices. All figures, tables, and equations shall be numerated. The original contribution of the candidate and material taken from other sources shall be clearly identified. Work from other sources shall be properly acknowledged using a Harvard citation style (e.g. DCU). Any plagiarism is taken very seriously by the university, and any such practice will have consequences. NTNU can use the results freely in its research work, unless otherwise agreed upon, by properly referring to the work.

The thesis shall be submitted in 2 printed copies, each signed by the candidate. The final revised version of this project description must be included. The report must appear in a bound volume or a binder according to the NTNU standard template. Computer code and a PDF version of the report should be included electronically.

A 15 min. presentation (conference style) should be given on your main results at time around delivery.

Start date: 1 February, 2011 **Due date:** As specified by the administration.

Supervisor: Professor Roger Skjetne
Co-advisor(s): Professor Sveinung Løset and Ph.d. stud. cand. Ulrik Jørgensen

Trondheim, February 2nd, 2011

_____

Roger Skjetne
Supervisor

Abstract

The purpose of this thesis is to develop a control scheme for the Arctic Multipurpose Vessel Oil Spill Fighter vessel model using a joystick as the connection between vessel and operator. A mathematical model of the vessel is also to be developed using data gathered from experiments done with the vessel model and existing maneuvering model theory. The parameters that are not determined during experiments have all been given an assumed value. The developed mathematical model is, in addition to providing the platform on which to test the controls, meant to be a framework ready for more accurate parameters done by future students.

The Oil Spill Fighter is an amphibious vessel powered by two Archimedes screws that run the length of the vessel on each side of the hull. This is not a unique way of powering an amphibious vessel, but no research have been found on the topic of how such a vessel moves on neither land nor water. This will therefore be discussed in this thesis. The results of this discussion will be appended to the mathematical model of the vessel in order to end up with a model as close to reality as is possible with the determined parameters.

In order to determine what control scheme to pursue, the work space and configuration space of the vessel are discussed. The conclusion of this discussion is to make the land-based control an open-loop control with the joystick providing surge force and yaw moment and the water-based control an autopilot. Those two controllers are then combined to come up with a single model of the amphibious property of the vessel.

When designing the controllers they are kept separate at first in order to simplify the design and tuning. The performance of each is presented and discussed separately and they are then combined into one model. The performance of this combined model is then presented.

The concept of hardware-in-the-loop testing is given an introduction, and the use of this type of testing with regards to the developed models are presented. This involves designing an interface in LabView which is connected to a CompactRIO that holds the model. The concept of real-time calculations are discussed, and a presentation of the developed models performance when uploaded to a CompactRIO and tested in the LabView interface is given. At the end the mathematical model is compared to the results from the experiments. These fit very well, and this result is discussed.

Contents

List of Figures

Preface

I would like to thank my supervisor Professor Roger Skjetne and my co-advisors Professor Sveinung Løset and Ph.D. student Ulrik Jørgensen for their aid and assistance during this work. I would especially like to thank Ulrik for taking the time to both assist in the laboratory testing and helping in brain storming for solutions. Thanks to Morten and Petter Scharffscher at M-Tech for lending me the model of the vessel for testing, and for being very helpful whenever I had a question or required aid. Thanks to Torgeir Wahl at MCLab for his willingness to share his experience and his invaluable help in configuring the equipment for my experiments. My parents are to be thanked for their efforts in proof-reading my thesis. And last, but not least, my fellow students. Thanks for all the games of table tennis throughout the year.

My time as a student comes to an end, and when this thesis is delivered I may finally call my self a Master of Science.

Writing a thesis such as this has been very different from the way I have worked up till now. No exercises due each week. No lectures. Being, more than ever, responsible for your own performance. It has been difficult to set and keep deadlines of my own, and to realize when I have spent too much time working on something that proves to be of little importance to the finished project. There have been times where my motivation have fallen, and times when I have been close to panic when my model started to act strangely (usually after I unwittingly changed something). But in the end I still find the subject of cybernetics extremely fascinating, and to quote the author Terry Pratchett: "It's still magic even if you know how it's done."

Chapter 1

Introduction

This thesis will deal with modelling and controlling the Arctic Multipurpose Vessel (AMV) Oil Spill Fighter (OSF), hereafter referred to as the OSF or the AMV OSF, conceived and built by Team Innovation Trondheim (TIT).

1.1 About the AMV OSF

The AMV OSF is an amphibious vehicle able to operate in areas unreachable to normal boats or vehicles. The vessel can navigate in very shallow waters, and safely overcome obstacles such as reefs or sunken rocks. The OSF is able to do this because of the two screws running on each side, and the entire length, of the vessel. These screws, in addition to providing the main source of buoyancy, rotate to move the vessel both on land and water.

The OSF was originally intended to be used as a lifeboat for offshore installations in arctic regions, the idea being that a lifeboat in these conditions needs to be able to handle ice. This did however require a lot of work to meet the strict health and safety requirements for operations in these regions. In order to fund the development, the vessel was presented to the oil protection organization NOFO (Norsk Oljevernsforening For Operatørselskap) as an amphibious platform, with remote control capabilities, that could be configured to a variety of tasks. NOFO was interested and decided to fund the development on the condition that the vessel was made slender enough to be legal to transport on a tailer. This was agreed upon and work on a full-scale prototype began.

1.1.1 Description of model vessel

Before any work started on the full-scale vessel, the model used during testing in this thesis was made. It was made to be able to show possible investors as a proof of concept. There are therefore some differences between the two. The full-scale vessel is, for instance, not a scaled-up version of the model. If the model were to be scale up to the same width as the full-scale vessel, the model would be about twice as long. Given that the length of the screws are equal to the length of the vessel, this has implications on the performance. The screws are not the same either. After considering the results presented in Engelbreth

(2009) it was decided to construct the full-scale vessel with two threads along each screw instead of the one which is used on the model. The pitch of this thread however is the same for model and full-scale vessel. A screw thread is a ridge wrapped around a cylinder in the form of a helix. The model vessel is made up of very basic geometric shapes, which will be utilized later in simplifying otherwise complex calculations.

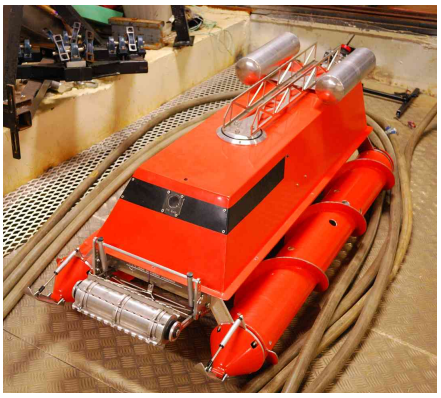

Figure 1.1: Vessel model

For a more detailed discussion of the vehicle and its uses and limitations, see chapter 1, 2 and 3 in Nilsen (2010).

1.1.2 History of the Archimedes screw

The inventor of what we know as the Archimedes screw is lost in history, however historians gives credit to the Greek philosopher Archimedes (circa 287-212 B.C.). Archimedes himself does not mention this device in any of his surviving texts, but Greek historians whose recordings begin around one hundred years after Archimedes claim he conceived it. According to said history, he invented it as a way to pump water out of ships which, due to the ship building technology available to the builders of the day leaked constantly. The introduction of a more effective way to remove this water made it possible to build larger ships. It works by encasing a screw in a cylinder, making sure that the screw fit as closely as possible, and putting one end in a source of water. Rotating the screw will move the water towards the other end, and placing this over some area where it can be safely deposited, results in an effective way of draining an area. The Archimedes screw is still for pumping today, both for water and as a gentle and effective way of transporting grain or other granulated material. See Rorres (2000) for more information on the history, present day use and design criteria for present use of the Archimedes screw.

With the steam engine, new methods of ship propulsion were being explored. Since the Archimedes screw was already a tried and tested method of moving water, the idea was to take away the tube previously surrounding it, attach it to a vessel, and see if it would provide enough thrust to propel it forward. This turned out to be a success, and the hunt for a more effective screw resulted in what we now know as the propeller, or the screw-propeller as it is usually referred to. It is for this reason that in propeller theory literature, the Archimedes screw is referred to as the origin of modern propeller design. The screws used by the OSF will be discussed in more detail later.

A few attempts to use the Archimedes screw to make an amphibious vessel have been made. During initial research for this thesis, presented in Nilsen (2010), vehicles such as the American Fordson snow machine from the 1920s and the Russian ZIL-2906 were found. No reasoning for why they were taken out of production has been found, but with regards to their intended use as all-terrain vehicles that could cope with marches and bogs it is suspected that they were replaced by caterpillar type vehicles and helicopters.

1.1.3 Uses for the OSF

If none of the previous attempts to make an Archimedes screw propelled vehicle has survived, why could the OSF be a viable product? With global demand for oil growing, and easily accessed reserves of oil becoming more and more scarce, the pressure to start drilling in arctic areas is growing. For this to be possible a lifeboat capable of operating in the arctic, during all seasons, is needed. The intention of the OSF is, as has been mentioned, just this. The problem introduced by ice that is threatening normal propeller powered vessels are ice preventing the inflow to the propeller, or the ice being too thick to crush by the vessels hull. This is solved by the screws which allow the vessel to pass through ice slush or over a sheet of ice given that the edge between ice and water is not to high.

In an oil spill situation, effective damage reduction and clean up requires a lot of equipment such as booms for containment and transportation of the gathered waste. The most used fuel for large ships today is bunker oil, of which these ships carries hundreds of tons. This type of oil is very heavy and viscous and therefore difficult to clean up effectively, so even when a vessel that is not an oil-tanker hits a reef or runs aground there is a real risk of a considerable oil spill. Since it is impossible to know where this may happen, one can not rely on easy access to the site of the accident. Here is where the OSF can be of use, since it can be deployed from any nearby road and can be used to transport in the equipment needed as well as partake in the cleanup process by laying containment booms.

See Nilsen (2010) for a more thorough discussion on the possible uses.

1.2 Objective

The objective of this thesis is to construct a joystick control system for the AMF OSF and design an environment based on experimental measurements in which to test it. Both these aspects are important. A good model is required for a good replication of the real vessel and a good controller is required if you want to use the model to test performance. The model can however be used for more than testing controllers. It can be used as a state estimator to both improve controller performance and also provide a dead reckoning capability which means that the control algorithm will be capable of handling the loss of one or more sensors. If, for example, the compass stops working and no data on the actual heading of the vessel is available, the state estimator can use the input parameters to estimate the actual heading. This estimate will deteriorate over time as the estimator will never be a perfect rendition of the real world, but the better the model the better the estimator. Dead reckoning is used as a safety precaution and is meant to allow the

operator the necessary control to move it to a safe place, or to safely end any ongoing operations.

1.2.1 Experiment

The experiments performed with the current model of the vehicle has been plagued with difficulties and setbacks. There are several reasons for this. One is that the model was made to be a showpiece. It was made to sell the idea of the AMV OSF. This means that it had to be made quite complex in order to house all the different ideas the designers had regarding obstacle handling as well as general movement. The screws are the prime movers, but the model contained a system for getting over humps that would normally get under the model and lift it up so that the screws did not get the traction needed. This was a system built to show possible investors that the problem had been given some thought, but it is not implemented on the full-scale prototype. The presence of this system on the model resulted in three, for the purpose of experimental tests of the screws, unnecessary holes in the hull under the waterline to house the drive shafts to this system. It also meant that the surge damping coefficients determined for the model would not be comparable to the coefficients of the full-scale vehicle, since the entire bottom plate of the model was made to hold this system. Because of the holes for the drive shafts the model leaked quite a lot of water and had to be made waterproof with silicone.

1.3 Outline

This chapter has been a short summary of my project of last semester. The next chapter will describe the mathematical model and the parameters used to describe the movement of the vessel. In chapter three some of these parameters will be determined as a result of testing. Chapter four will discuss a joystick control design, and in chapter five an autopilot design will be presented. In chapter six the combined land and water model will be described and discussed. Chapter seven introduces Hardware-in-the-loop testing and the validation of the model presented in this theses. The last chapter will be the conclusion and further work.

Chapter 2

Modelling the AMV OSF

In this section, the mathematical model of the OSF is presented and explained. Obtaining a good mathematical model of a vessel is important for obtaining a good control design, and will also aid understanding the vessels movements. The standard model for marine vessels is defined for six degrees of freedom (DOF), DOFs will be discussed in the following section, and the equations also include how these six degrees are connected to each other. This results in a total of 36 equations that will, with perfect parameters, describe all possible movements of the vessel with a high degree of accuracy. We can however disregard several of these equations when working on a subset of all possible movements. The model used is taken from Section 3.5 in Fossen (2010) and is

$$\dot{\boldsymbol{\eta}} = \mathbf{R}(\psi)\boldsymbol{\nu} \tag{2.1}$$

$$\mathbf{M}_{RB}\dot{\boldsymbol{\nu}} + \mathbf{M}_{A}\dot{\boldsymbol{\nu}} + \mathbf{C}_{RB}(\boldsymbol{\nu})\boldsymbol{\nu} + \mathbf{C}_{A}(\boldsymbol{\nu})\boldsymbol{\nu} + \mathbf{D}(\boldsymbol{\nu})\boldsymbol{\nu} = \boldsymbol{\tau} + \boldsymbol{\tau}_{wind} + \boldsymbol{\tau}_{wave}. \tag{2.2}$$

These equations will be explained in detail in this chapter.

2.1 Reference frames

A reference frame gives information on how an observed object move in relation to a given point. Before we start presenting the model itself we need to introduce the different reference frames used to denote position and speed. There are two frames used in this text. Body-fixed and geographical, and in marine terminology the axis of these frames are given other names than the normal x, y and z. The difference between the two frames is the following figure.

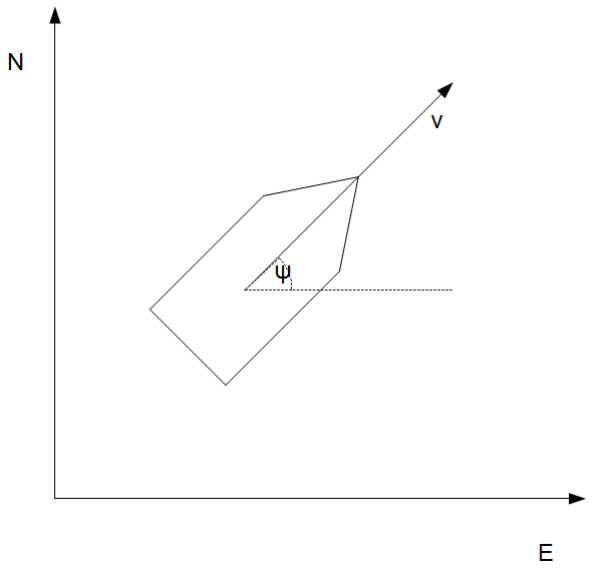

Figure 2.1: Geographical/body-fixed reference frame

The geographical reference frame is often called the NED-frame and it is common to orientate the frame so that the x-axis points to north and the y-axis points to east. The z-axis then points down, as it is common in calculations involving water to define the surface of the water as $z = 0$ and the bottom as $z = -waterdepth$. The body-fixed frame is a moving frame fixed to the vessel. The transformation of one reference frame to another is presented later. The reference frames denote position and motion in six degrees of freedom (DOF), made up of the three dimensions of the Cartesian coordinate system and the rotation around these dimensions. The six DOFs can be separated into three horizontal and three vertical DOFs.

2.1.1 Body-fixed frame

The body-fixed reference frame is placed with its origin in a specific location on the vessel, usually midship on the waterline. It will rotate and move with the vessel and because of this, offer no direct information on the geographical position of the craft. The body-fixed reference frame shows the velocity vector of the vessel as seen by the vessel.

$$\boldsymbol{\nu} = \begin{bmatrix} \mathbf{v}^b_{b/n} \\ \boldsymbol{\omega}^b_{b/n} \end{bmatrix} = \begin{bmatrix} u & v & w & p & q & r \end{bmatrix}^T \tag{2.3}$$

These speeds and rotations here are in marine terminology referred to as

Symbol	Name
u	surge
v	sway
w	heave
p	roll
q	pitch
r	yaw

2.1.2 Geographic reference frame

The geographic reference frame is defined as a fixed position relatively close to the vessel. Because of the curvature of the earth, the distance between the origin and the vessel can not be too great since the horizontal velocities of the vessel is tangential to the earth surface and a great distance will result in an angle between actual velocity and the velocity that the frame observes. Thus a new origin will need to be specified if the vessel moves too far. The geographic reference frame shows the position of the vessel as seen by the origin of the frame.

$$\boldsymbol{\eta} = \begin{bmatrix} \mathbf{p}_{b/n}^{n} \\ \boldsymbol{\Omega}_{nb} \end{bmatrix} = \begin{bmatrix} N & E & D & \phi & \theta & \psi \end{bmatrix}^{T} \tag{2.4}$$

2.1.3 Notation

Cartesian	body-fixed (velocity)	NED (position)
x	u	N
y	v	E
z	w	D
ϕ	p	ϕ
θ	q	θ
ψ	r	ψ

2.2 Work space vs. configuration space

In the previous section we defined the reference-frames to be used in modelling the vessel. These frames both describe position and motion in 6 degrees of freedom where there are three horizontal (surge, sway and yaw) and three vertical (heave, roll and pitch). When we want to control any vessel or vehicle, we need to define which of these DOFs the vessel can use to achieve a desired task, and which DOFs are available to the vehicle to achieve this task. This then determines whether the vessel is fully actuated or underactuated, where a fully actuated vessel can control its movement in all the DOFs it is designed to operate in. An underactuated vessel is a vessel which lacks one or more controllable DOF.

The two following definitions are taken from Section 9.4 in Fossen (2011):

> Configuration space: The n-dimensional configuration space is the space of possible positions and orientations that a craft may attain, possibly subject to external constraints. The configuration of a marine craft can be uniquely described by an n-dimensional vector of generalized coordinates that is the least number of coordinates needed to specify the states of the system.
>
> Workspace: The workspace is a reduced space of dimension m<n in which the control objective is defined. The workspace of a conventional heading autopilot is m=1 since only the yaw motion is controlled. Similarly, the workspace of a horizontal plane controller, for instance a DP system controlling the motion in surge, sway and yaw, is m=3.

The screws propelling the OSF are fixed, meaning that they can not change the angle of the produced thrust. Because they are placed a distance from the rotational center, they do produce a moment and this is how the OSF changes heading. The configuration space is therefore made up of the two degrees of freedom surge and yaw. A more thorough presentation of the screws will be done later. Using these DOFs the OSF is capable of reaching any point described by the workspace, but not directly. This holds on both land and water, with the added possibility of sideways, sway, motion if there is not enough grip for the screws. The control objective in both cases will be to control as many DOFs as possible.

According to the definitions above, the configuration space for an autopilot is three-dimensional and made up of the horizontal DOFs surge, sway and yaw. The workspace is one-dimensional since the only DOF needed to meet the control objectives is yaw. If surge speed control is added, this then becomes two-dimensional.

The configuration space On land is three-dimensional, the same as for water. This is because we in both cases operate on the horizontal DOFs. The workspace on land is divided into two parts since we have two distinct control objectives. One is control in surge and yaw control, and the other is control in sway. A more detailed discussion on movement on both land and water will follow.

2.3 3-DOF rigid body dynamics

The rigid body dynamics describe the Newtonian forces acting on the vessel during acceleration. According to Newton's Second Law, mass times acceleration equals force. Newton's First Law specify that when the velocity is unchanging, no force acts on the system, while his third law states that an object exerting a force on another object will in turn be effected by a counterforce of equal magnitude. These laws were published in 1687 by Isaac Newton (1643-1727) in his "Philosophia Naturalis Principia Mathematica", and are the basis for establishing the rigid body dynamics of a vessel. A vehicle operating on water is free to move in both horizontal directions, N and E, as well as rotate around the vertical axis D. Because of these three degrees of freedom we need to calculate the Newtonian force acting on the vessel in x and y direction, as well as the angular. However, we can state the form of the equation before determining its parameters. Here, the rigid body dynamics presented in Section 3.1.3 in Fossen (2010) is used.

$$\begin{aligned} \dot{\boldsymbol{\eta}} &= \mathbf{R}(\psi)\boldsymbol{\nu} \\ \mathbf{M}_{RB}\dot{\boldsymbol{\nu}} + \mathbf{C}_{RB}(\boldsymbol{\nu})\boldsymbol{\nu} &= \boldsymbol{\tau}_{RB} \end{aligned} \tag{2.5}$$

where $\mathbf{M}_{RB}$ is the rigid body mass, $\mathbf{C}_{RB}(\boldsymbol{\nu})\boldsymbol{\nu}$ is the rigid body Coriolis matrix and $\boldsymbol{\tau}_{RB}$ is the vector of forces acting upon the system defined as

$$\boldsymbol{\tau}_{RB} = \boldsymbol{\tau}_{hyd} + \boldsymbol{\tau}_{hs} + \boldsymbol{\tau}_{wind} + \boldsymbol{\tau}_{wave} + \boldsymbol{\tau} \tag{2.6}$$

where $\boldsymbol{\tau}_{hs} = 0$ in the horizontal 3DOF plane. $\boldsymbol{\tau}_{hyd}$ are the hydrodynamic forces discussed later. $\boldsymbol{\tau}_{waves}$ and $\boldsymbol{\tau}_{wind}$, and also $\boldsymbol{\tau}_{current}$ which may be included, make up the environmental forces that are grouped under the term bias forces. The $\boldsymbol{\tau}$ term holds the forces

produced by the thrusters. The matrices and vector of the rest of the equation have the following form.

$$\boldsymbol{\nu} = \begin{bmatrix} u \\ v \\ r \end{bmatrix} \tag{2.7}$$

$$\mathbf{M}_{RB} = \begin{bmatrix} m & 0 & -my_g \\ 0 & m & mx_g \\ -my_g & mx_g & I_z \end{bmatrix} \tag{2.8}$$

$$\mathbf{C}_{RB}(\boldsymbol{\nu}) = \begin{bmatrix} \mathbf{0}_{3\times 3} & -m\mathbf{S}(\mathbf{M}_{11}\boldsymbol{\nu}_1 + \mathbf{M}_{12}\boldsymbol{\nu}_2) \\ -\mathbf{S}(\mathbf{M}_{11}\boldsymbol{\nu}_1 + \mathbf{M}_{12}\boldsymbol{\nu}_2) & -\mathbf{S}(\mathbf{M}_{21}\boldsymbol{\nu}_1 + \mathbf{M}_{22}\boldsymbol{\nu}_2) \end{bmatrix} \tag{2.9}$$

$$= \begin{bmatrix} 0 & 0 & -m(x_g r + v) \\ 0 & 0 & mu \\ m(x_g r + v) & -mu & 0 \end{bmatrix} \tag{2.10}$$

These will be discussed shortly.

2.3.1 Kinetics

In Section 2.1, the reference frames used in the model were introduced. In order to be able to use both frames in our equations we need to specify their relation to each other. As stated, the NED frame defined in Equation 2.4 is geographically fixed whereas the body-fixed frame defined in Equation 2.3. Thus, surge speed in the body frame will be translated into a change in both N and E position on the NED frame unless the surge direction is equal to either the defined N or E direction. This is illustrated in Figure 2.1. Since the model is defined using body-fixed coordinates we need to define an equation that transforms those coordinates into the NED frame in order to get information about the vessels position. We only look at the three horizontal DOFs which is a good simplification if you assume small changes in ϕ and θ.

This may not be a valid assumption as when the screws rotate they create forces that may lift the vessel, but for this case where we focus on surge, sway and yaw movements this assumption is made. The equation is

$$\dot{\boldsymbol{\eta}} = \mathbf{R}(\psi)\boldsymbol{\nu} \tag{2.11}$$

where

$$R(\psi) = \begin{bmatrix} \cos(\psi) & -\sin(\psi) & 0 \\ \sin(\psi) & \cos(\psi) & 0 \\ 0 & 0 & 1 \end{bmatrix} \tag{2.12}$$

which is called a rotation matrix where the x and y, or N and E, coordinates are rotated to a new angle. Here that angle is the heading of the vessel turning velocity given in the NED frame into velocity given in the body-fixed frame.

2.3.2 Rigid-body mass

Based on observations of the model floating in water, the center of buoyancy and the center of mass is assumed to be at the same location. This means that x_g and y_g in Equation 2.8 is assumed to be zero, and the mass matrix becomes purely diagonal.

The density of the vessel is needed for the I_z. The volume of the vessel is calculated to be $0.1450[m^3]$, and the weight has been roughly measured to 40kg. As stated above, we assume $x_g = 0$, so the center of mass is located at the geometrical center. We therefore assume the density of the vessel to be uniformly distributed. Thus, the density is $\rho_m = \frac{mass}{volume} = 276\frac{kg}{m^3}$. For caluclating the I_z, the following cross section simplifications is used.

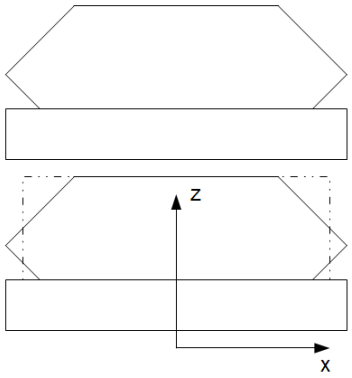

Figure 2.2: Moment of inertia cross section x-z

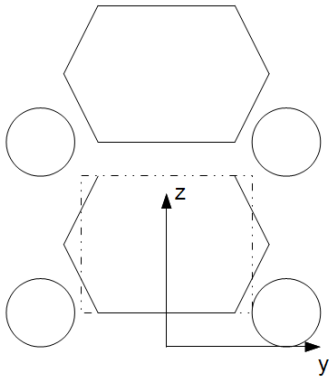

Figure 2.3: Moment of inertia cross section y-z

As seen from these figures, we simplify the shape of the model into 2 basic shapes. One box and two cylinders. The width of the box is 0.307m, the breadth is 0.308m and the length is 1.1m. The length of one cylinder is 1.17m and the radius is 0.074m. The bottom of the box is 0.04m below the top of the cylinders. Using this and the parallel axis theorem presented in section 18.4 in Irgens (1979), we can determine I_z. The parallel axis theorem states

$$I_z = I_{cm} + md_z^2 \tag{2.13}$$

where I_{cm} is the moment of inertia for one object around an axis passing through its center of mass, m is the mass of that object and d_z is the distance between the objects center

of mass and the entire structures center of mass in the z direction. The total moment of inertia is then the sum of these individual I_z values. With regards to the assumption that $x_g = 0$ and the simplifications shown previously, we can say that the center of the vessels mass is through the center of the box that is the main body, and the entire model is symmetrical along both x and y axis. The resulting equation is then

$$I_{z,total} = I_{cm,box} + m_{box}d^2_{z,box} + 2(I_{cm,cylinder} + m_{cylinder}d^2_{z,cylinder}). \tag{2.14}$$

Here, z is the position of the whole structures center of mass on the z-axis. To identify the z parameter, we first define the bottom of the screw as $z = 0$ and the center of the box as $x = y = 0$. The center of mass for the cylinder is placed in the center of the cylinder, i.e. $z_{cylinder} = 0.074m = radius$. The center of mass for the box is the center of the box, making $z_{box} = 0262m$. Knowing the volume of each object and the density of the model we can then find the z value for the center of mass by looking at a cross section of the structure in $x = y = 0$.

$$z = \frac{\rho_m A_{box} z_{box} + \rho_m 2A_{cylinder} z_{cylinder}}{276(A_{box} + 2A_{cylinder})} = 0.2118 \tag{2.15}$$

The two different I_{cm} are

$$I_{cm,box} = \frac{1}{12}\rho_m V_{box}(w^2 + b^2) \tag{2.16}$$

$$m_{box}d^2_{z,box} = \rho_m V_{box}(z^2_{box} - z^2) \tag{2.17}$$

$$I_{cm,cylinder} = \frac{1}{12}\rho_m V_{cylinder}(3r^2 + l^2) \tag{2.18}$$

$$m_{cylinder}d^2_{z,cylinder} = \rho_m V_{cylinder}(z^2_{cylinder} - z^2) \tag{2.19}$$

where w is the width of the box, b is the breadth of the box, r is the radius of the cylinder and l is the length of the cylinder. The component values are then

- $I_{cm,box} = 3.12$
- $m_{box}d^2_{z,box} = 0.072$
- $I_{cm,cylinder} = 0.641$
- $m_{cylinder}d^2_{z,cylinder} = 0.106$

resulting in $I_z = 4.684$. As previously stated, the mass of the vehicle is 40kg. The rigid-body mass matrix then becomes

$$M_{rb} = \begin{bmatrix} 40 & 0 & \\ 0 & 40 & 0 \\ 0 & 0 & 4.684 \end{bmatrix} \tag{2.20}$$

2.3.3 Rigid body Coriolis effect

The Coriolis/centripetal forces are forces introduced into the equation by transforming a body-fixed reference frame into a geographic one. A thought-experiment can be useful in

order to see why this is necessary. Imagine a horizontal circular disk rotating around its own axis. Now imagine picking up a marble and rolling it, starting on one edge, through the center, and off the opposite edge. If viewed while standing above, looking down on the spinning disk, the movement will be in a straight line. However, if we imagine we view it from the edge of the spinning disk at the point where the marble enters the disk, one would observe that the marble leave the disk at a place different than the opposite edge which it was heading for. Some force seems to have pushed it off course. This is the Coriolis/centripetal force.

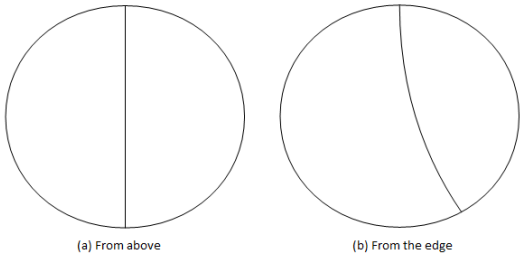

Figure 2.4: Coriolis effect visualized

The effect this has on a mathematical model is that it provides the connection between yaw moment and forces in surge and sway, so that a constant yaw moment results in the vessel moving in circles instead of just changing heading.

2.4 Hydrodynamics

The hydrodynamics describes the forces acting on a vessel moving in water. When developing a mathematical model of a vessel it is the parameters of these equations that demand the most attention. It does not take a big increase in velocity for non-linear effects to dominate, and the specific increase is depending on the hull design. The OSF is not designed to be hydrodynamical effective, and the rotating screws that make up a big part of the hull makes it quite difficult to determine the effects.

The velocity of the vessel is very important in hydrodynamics. When a vessel moves through water, the velocity of the vessel defines the resistance induced by the incoming water. If there is a water current present the velocity of this current is added to the velocity of incoming water, since the vessel feels a resistance equal to moving faster than the actual velocity. This is called the relative velocity and is denoted $\boldsymbol{\nu}_r = \boldsymbol{\nu} - \boldsymbol{\nu}_c) = [u - u_c, v - v_c, r]^T$. If the current follows the vessel speed it is evident from the $\boldsymbol{\nu}_r$ definition that the resistance is lower than for the same speed in still water. The hydrodynamics part of the system equation, Equation 2.2, is

$$\begin{aligned} \dot{\boldsymbol{\eta}} &= \mathbf{R}(\psi)\boldsymbol{\nu} \\ \mathbf{M}_A\dot{\boldsymbol{\nu}}_r + \mathbf{C}_A(\boldsymbol{\nu}_r)\boldsymbol{\nu}_r + \mathbf{D}(\boldsymbol{\nu}_r)\boldsymbol{\nu}_r &= -\boldsymbol{\tau}_{hyd}. \end{aligned} \tag{2.21}$$

Note that if we insert this into Equation 2.5 we get Equation 2.2. The terms in this

equation is

$$M_a = \begin{bmatrix} A_{11} & A_{12} & A_{16} \\ A_{21} & A_{22} & A_{26} \\ A_{61} & A_{62} & A_{66} \end{bmatrix}, \tag{2.22}$$

$$\mathbf{C}(\boldsymbol{\nu}) = \begin{bmatrix} \mathbf{0}_{3\times 3} & -\mathbf{S}(\mathbf{M}_{11}\boldsymbol{\nu}_1 + \mathbf{M}_{12}\boldsymbol{\nu}_2) \\ -\mathbf{S}(\mathbf{M}_{11}\boldsymbol{\nu}_1 + \mathbf{M}_{12}\boldsymbol{\nu}_2) & -\mathbf{S}(\mathbf{M}_{21}\boldsymbol{\nu}_1 + \mathbf{M}_{22}\boldsymbol{\nu}_2) \end{bmatrix} = \begin{bmatrix} 0 & 0 & Y_{\dot{v}}v + Y_{\dot{r}}r \\ 0 & 0 & -X_{\dot{u}}u \\ -Y_{\dot{v}}v - Y_{\dot{r}}r & X_{\dot{u}}u & 0 \end{bmatrix}, \tag{2.23}$$

and

$$\mathbf{D}(\boldsymbol{\nu}_r) = \mathbf{D} + \mathbf{D}_n(\boldsymbol{\nu}_r) \tag{2.24}$$

$$\mathbf{D} = \begin{bmatrix} -X_u & 0 & 0 \\ 0 & -Y_v & -Y_r \\ 0 & -N_v & -N_r \end{bmatrix} \tag{2.25}$$

$$\mathbf{D}_n(\boldsymbol{\nu}_r) = \begin{bmatrix} -X_{|u|u}|u_r| & 0 & 0 \\ 0 & -Y_{|v|v}|v_r| - Y_{|r|v}|r| & -Y_{|v|r}|v_r| - Y_{|r|r}|r| \\ 0 & -N_{|v|v}|v_r| - N_{|r|v}|r| & -N_{|v|r}|v_r| - N_{|r|r}|r| \end{bmatrix}. \tag{2.26}$$

These equations will be discussed in the following text.

2.4.1 Added-mass effect

Added mass can be thought of as a virtual weight added to the system because of the water an accelerating or decelerating object has to move as the object and the fluid cannot occupy the same physical space simultaneously.

The importance of added mass can be seen in a simple thought experiment taken from Greco (2010). We imagine an air bubble immersed in infinite water is released at t=0. The bubble has volume V. The air density $\rho_0 = 1.21\frac{kg}{m^3}$ and the water density is $\rho = 998.2\frac{kg}{m^3}$. It is known from fluid mechanics that the buoyancy and weight of the bubble will be $\rho V g$ and $\rho_0 V g$, respectively, where g is the acceleration of gravity. If we denote $\ddot{\eta}_3$ as the acceleration the bubble will experience upwards through the fluid, we can say

$$\rho_o V\ddot{\eta}_3 = (\rho - \rho_0)Vg \implies \ddot{\eta}_3 = \frac{\rho - \rho_0}{\rho_0} g \approx 800g. \tag{2.27}$$

That is, the bubble will accelerate at 800 times the speed of gravity. This is of course impossible. If we add the effect from added mass with the term $F_3 = -A_{33}\ddot{\eta}_3 = -0.5\rho V\ddot{\eta}_3$, where A_{33} is the added mass in heave direction, we see that

$$(\rho_o V + 0.5\rho V)\ddot{\eta}_3 = (\rho - \rho_0)Vg \implies \ddot{\eta}_3 = \frac{\rho - \rho_0}{\rho_0 + 0.5\rho} g \approx 2g. \tag{2.28}$$

This seems much more realistic. For calculating the added mass of the model vessel, the following submerged y-z cross-section was used.

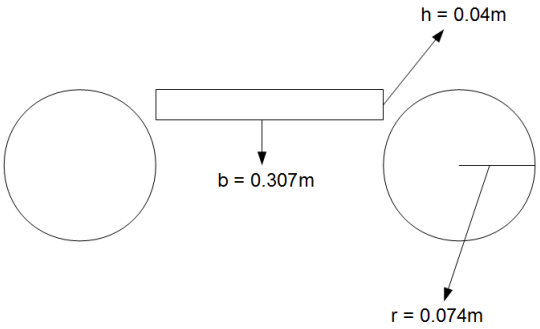

Figure 2.5: Added mass calculation

The circles have a radius of 0.074m, while the box is 0.307m wide and 0.308m high resulting in the area of the each circle is $0.0172m^2$ and the area of the recangle is $0.0946m^2$, with a total area of $A_s = 0.129m^2$. Using the theory and equations presented in page 41-56 in Faltinsen (1990), we begin with calculating the two-dimensional added mass for the cross section.

$$A_{22}^{(2D)} = A_s * \rho. \tag{2.29}$$

This is then used to determine the three-dimensional added mass.

$$A_{22} = \int_L A_{22}^{(2D)}(x)dx$$
$$A_{26} = -\int_L xA_{22}^{(2D)}(x)dx$$
$$A_{66} = \int_L x^2A_{22}^{(2D)}(x)dx$$

where ρ is the density of the medium the structure moves in, in this case fresh water which has a density of $1000\frac{kg}{m^3}$. Since the added mass matrix is symmetrical, A_{62} is the same as A_{26}.

On ships with complex hull shape, Strip Theory is used to get the three-dimensional added mass. This involves splitting the hull into sections and calculate the 2D added mass for each section. The sum of all those 2D added mass elements is then the 3D added mass. The higher number of sections will then equal higher accuracy of the resulting added mass, but will in turn demand more time to calculate. The theory in Faltinsen (1990) recommends using 10 sections for normal hull types. The OSF can be simplified to very basic geometric shapes, as seen in Figure 2.2 and Figure 2.3, without loosing much accuracy, so in this case this will not be used. Calculating the 2D added mass over the cross section of the vessel and integrating along the length is considered to be accurate enough to roughly replicate the vessels hydrodynamic properties. Parameters calculated to be

- $A_{22}^{2D} = 46.78$
- $A_{22} = 51.4$
- $A_{26} = 28.2$
- $A_{62} = A_{26}$
- $A_{66} = 20.7$

Strip theory works on the assumption that the velocity of the water is uniform along the contour of one strip when the vessel moves in surge direction and no current is present. When the strip is based on the y-z cross section of the vessel this assumption holds, however using strip theory to find added mass in the surge direction introduces some problems. The cross section is now based on the x-z plane, and the assumption that the velocity of the water is uniform along this contour is invalid. Since the water flows along the hull in surge direction, the water flow is given the entire length of the vessel to be influenced by drag introduced by the hull surface. Vortexes will appear and the shape of the hull itself may divert the flow. Because of this, $A_{11} = 10$ is assumed.

2.4.2 Added mass Coriolis effect

The Coriolis/centripetal effect appears for the added mass for the same reason as it does for rigid-body mass.

2.4.3 Damping

The hydrodynamic damping affecting a marine craft are mainly caused by potential damping, skin friction, wave drift damping, damping due to vortex shedding and lifting forces. See Fossen (2010) for details about each damping effect. When designing a mathematical model of a vessel, these factors are usually superpositioned into

$$\mathbf{D}(\boldsymbol{\nu}_r) = \mathbf{D} + \mathbf{D}_n(\boldsymbol{\nu}_r) \tag{2.30}$$

where $\mathbf{D}$ is the linear damping due to potential damping and skin friction, and $\mathbf{D}_n(\boldsymbol{\nu}_r)$ is the nonlinear damping due to higher order terms. When determining the damping parameters it is important to note that the purpose of the damping is remove energy from the system. The parameters then have to be strictly positive, $\mathbf{D}(\boldsymbol{\nu}_r) > 0$. If this is not the case, then the resulting velocities will never cease accelerating which is quite clearly wrong. The surge damping termed X will be identified later. The other parameters will be discussed after that in light of the identified surge damping.

2.5 Propulsion

The models propulsion comes from its two screws. These are powered by two electro motors which are connected, through a gear, to their respective screws with a cycle chain. Since the electro motors rotate very fast, the rotation needs to be geared down. This is because the power produced are limited by the motors, and the equation for torque shows $torque = \frac{power}{2\pi rps}$ shows that lower rps equals higher torque.

2.5.1 Propulsion on water

The allocation of the thrust generated by the screws can be visualized with the following figure.

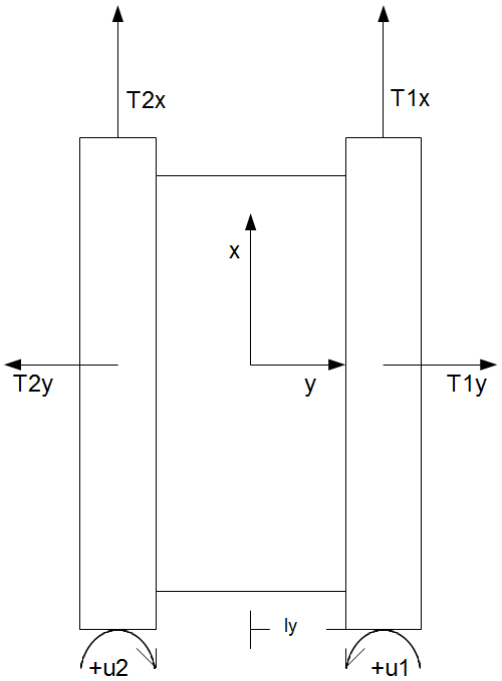

Figure 2.6: Thrust allocation

Where l_y is the distance between the resulting surge force generated by one screw and the geometric center of the vessel. Here it is measured as 0.22m. We can now define the thrust and moments in the body frame as

$$\tau_b = \begin{bmatrix} \tau_u \\ \tau_v \\ \tau_\psi \end{bmatrix} = \begin{bmatrix} T_{1x} + T_{2x} \\ T_{1y} - T_{2y} \\ 0.22(T_{1x} - T_{2x}) \end{bmatrix} \tag{2.31}$$

Note that the sway force is assumed to work uniformly along the length of the screw and thus will not contribute to the yaw moment as illustrated by the placement of the resulting sway force vector. If we look at the T_y forces we see that if the rotation of the screws are negative, the force will point in the opposite direction. In Nilsen (2010) it is argued that the T_y provided by the screws will always be in the same direction, away form the hull. This is because the screws are suspected to generate both a pressure difference around themselves and a sideways force from each thread on the screw. The presence of the hull is assumed to negate the forces directed towards it, and we end up with T_y being independent of the direction of rotation. This means that given the right control, one should be able to achieve sideways motion by sacrificing control over surge and yaw directions.

We now need to define the different thrusts as a function of the rotational speed u. It is a safe assumption that both screws generate the same amount of thrust given the same rotational speed. We use this to state the following:

$$\begin{aligned} \tau_u &= T_{1x} + T_{2x} = k_x u_1 + k_x u_2 = k_x(u_1 + u_2) \\ \tau_v &= T_{1y} - T_{2y} = k_y u_1 - k_y u_2 = k_u(u_1 - u_2) \\ \tau_\psi &= l_y(T_{1x} - T_{2x}) = l_y k_x(u_1 - u_2) \end{aligned} \tag{2.32}$$

which we can put on matrix form

$$\tau_b = TKu = \begin{bmatrix} 1 & 0 & 1 & 0 \\ 0 & 1 & 0 & -1 \\ l_y & 0 & l_y & 0 \end{bmatrix} \begin{bmatrix} k_x & 0 \\ k_y & 0 \\ 0 & k_x \\ 0 & k_y \end{bmatrix} \begin{bmatrix} u_1 \\ u_2 \end{bmatrix} \tag{2.33}$$

2.5.2 Propulsion in waves

Tests done in Engelbreth (2009) shows that there is little difference in the generated thrust for a fully submerged versus a half submerged screw. It is assumed that this is because the half submerged screw throws up a substantial amount of water when rotating at the speeds used for testing in that paper. Because the screws on the model used during experiments for this thesis is almost fully submerged, it is assumed that waves will not significantly reduce produced thrust when operating in waves. The worst case wave would be a singular sine wave with length and height equal the length and height of the screw as visualized in the figure below.

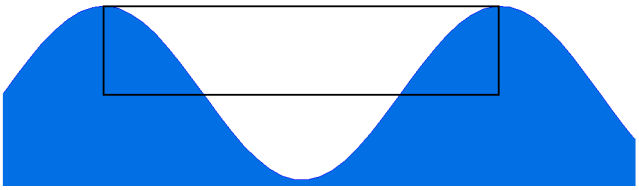

Figure 2.7: Screw in worst case wave

We see here that the mid section of the screw is not submerged. It is not known if the submergence shown in this figure is the actual submergence of the screw in such a wave. A speed reduction is suspected when moving in waves, but this would then have its source in the water moving inside the wave resulting water flowing in the opposite direction of the vessels movement.

2.5.3 Propulsion on land

This chapter has been focused on developing a mathematical model to describe movement on water. On land, only the rigid body model will be used. Movement and propulsion on land will be discussed in the chapter named Joystick control design.

Chapter 3

System Identification

The experiments were done at Marintek's Marine Cybernetics Laoratory (MCLab). It consists of a basin 6m wide, 40m long and 1.5m deep with a towing carriage and other equipment for simulating environmental forces and recording positions and forces. For the experiments done here, only the carriage and the force recorders are used. The forces measured by the sensors are recorded by a logger made by the company HBM called MGC+, and are sent to the logging program Catmat Professional Ver.5.0. The resulting measurements are used in a MatLab script to calculate the body-fixed forces and moments.

3.1 Testing objectives

With the goal of the thesis being the design of a joystick/autopilot control and an environment in which to test this, an important factor to determine is the thrust generated by the rotating screws. This will then be used to find the thrust coefficients which will be used later to replicate the results from the experiments. Testing the thrust was done by testing the bollard pull of the vessel. The bollard pull of a vessel is defined as the thrust that the vessel produces when prevented from moving. This means that there in theory will be no water flow around the thrusters which maximize the thrust. Thrust production in flowing water will be discussed later.

It is also of interest to find the damping coefficients in the relevant degrees of freedom. As has been discussed in Section 2.2, we are interested in surge, sway and yaw. Determining yaw damping is a quite complicated procedure involving rotating the vehicle around the z-axis while keeping it steady in the x- and y-axis, and measure the rotational speed of the vehicle along with the rotational speed of the screws. To achieve this with the model available for this thesis would take too much time away from more pressing matters, and the yaw damping is therefore given an assumed value. This will be discussed later. Surge damping is easier to determine and is included. Sway damping however is not. The setup would be the same for surge and sway damping, but time issues resulted in that part being omitted. This can in some way be justified by the suspicion that a big part of the sideways cross section of the vessel is made up of the screws, so the sway damping would be heavily depending on the screws rotational speed.

3.2 Setup and execution

There are three different test setups used, where two are setups for testing bollard pull. The reason for this is that the second experiment focused on purely surge force while the first was an attempt to find all the forces in one go which resulted in data difficult to interpret. To measure the rotation of the electro motors, two other electro motors were installed and connected to the first two with rubber bands. When the original motors rotated, the new motors would rotate and generate electricity. This output was measured and from it the rps was calculated.

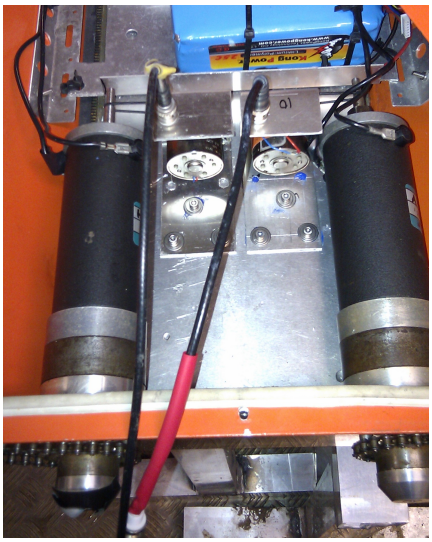

Figure 3.1: The rps sensors inside the model

The remote control used to control the OSF model had two levers that worked in one dimension, forward and backward. The left lever controlled the left screw and full forward on the lever meant full forward speed on the screw. The left lever was also in a way discrete in the sense that it had 12 notches in which the lever could be left standing. The right lever lacked these notches, and can therefore be called continuous. The right side was measured with a caliper gauge and the length divided by 12 to get as close as possible to duplicate the 12 notches on the left side. However, it was impossible to get the distance completely correct, so even for the runs intended with similar speed on both screws there is a slight difference.

The following explains the three tests done and presents the data they provided.

3.2.1 Fist bollard pull test

The model vessel needs to be prevented from moving. This is done by tying static ropes to anchor points on land and on the carriage. The vessel is placed in one end of the tank, with the bow pointing towards land. This means that the wake produced by the thrusters will have as much water as possible in which to develop naturally. In propeller theory, most calculations are done with the assumption that the wake has infinite water to develop freely so that the water flow does not stop abruptly and thus create pressure.

Infinite, or close to infinite, water is rarely the case, and in MClab the very limited depth of the basin will result in suboptimal wake. However, for this thesis, that is not something that will be taken into account.

A test performed to get an idea of how powerful the thrusters are, were performed and on full power a thrust of 60N was observed. This is by no means an accurate reading, but was a useful first impression. The setup for the first test is as follows.

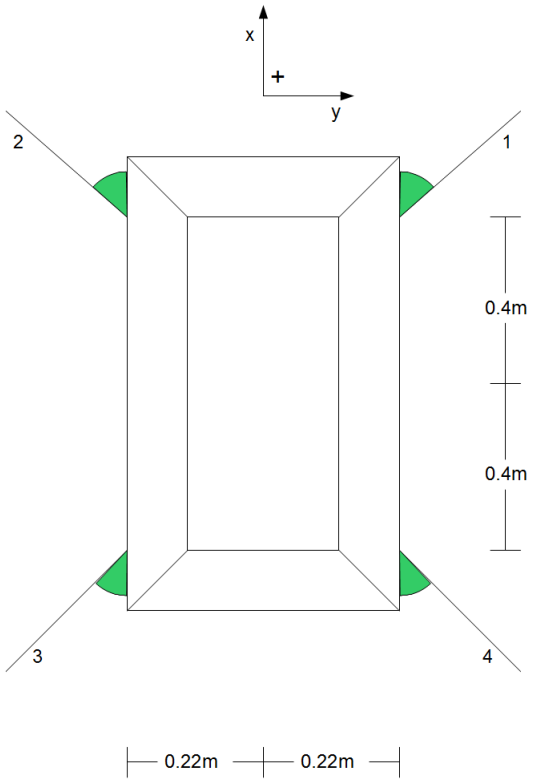

Figure 3.2: Experiment setup for first bollard pull test

Number	sensor number	angle
1	8121	24.5°
2	8111	155.5°
3	8114	228°
4	8110	307.8°

The angles are used to determine the x and y components of the measured force.

The test was executed by setting the holding the right lever in a fixed position while moving the left lever through the 12 notches mentioned above. The sensors logged the produced force and the screws rotational speed.

3.2.2 Second bollard pull test

This test differs from the first by including springs at the front two sensors in order to dampen any unwanted oscillation and to focus the measurement on the two sensors at the back, which then would measure all the forward force registered.

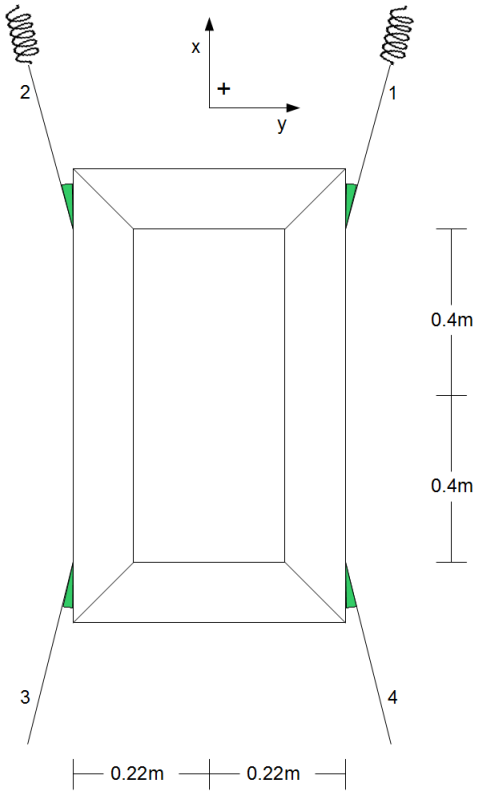

Figure 3.3: Experiment setup for second bollard pull test

Number	sensor number	angle
1	8114	59.8°
2	8116	120.3°
3	8111	250.7°
4	8113	289°

Again, the angles are used to determine the x and y components of the measured force.

This test was executed by trying to keep the screws rotational velocity equal. As mentioned above, this proved difficult to get perfectly correct, and a difference in velocity was unavoidable. However, this difference was quite small so the results were judged to be usable.

3.2.3 Surge damping test

The setup here is almost the same as in Figure 3.3. The sensors and angles are the same, and the only difference is that the springs are changed to the back two tethers. This

is done because it is impractical to spend time to get the model lined up straight, so the springs attached to the back two tethers make sure that the model keeps a straight heading when moving.

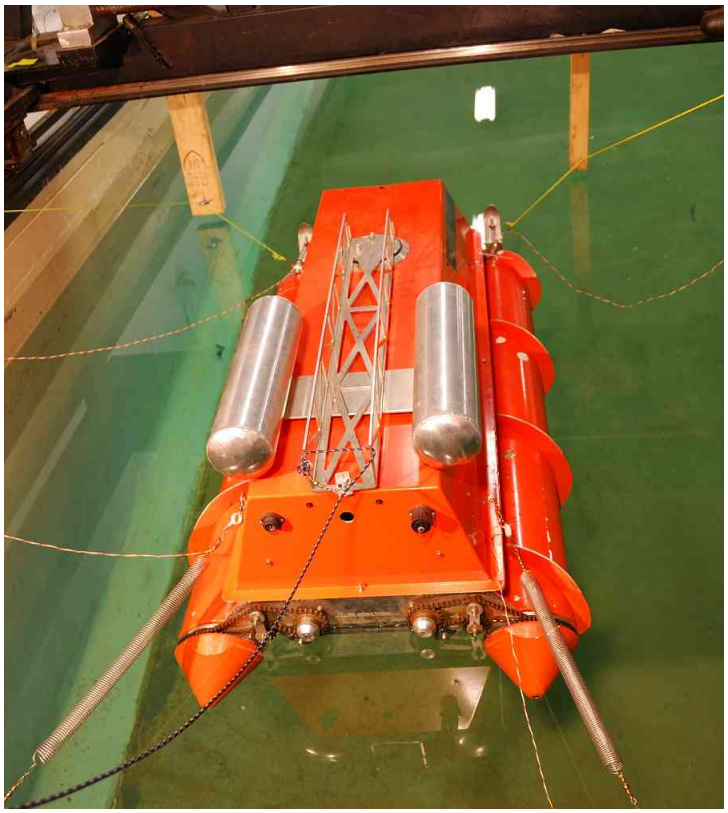

Figure 3.4: Experiment setup for second bollard pull test, photo

Note the boards that the model is fastened to. These were set up by student Håkon Skåtun for his experiments, and proved well suited for this test as well. The boards are there to make sure that the tether is kept as horizontal as possible. This photo shows the setup used for the second bollard pull test as well, but with the springs in different location.

When executing the experiment the model was fastened to the carriage which was set to move forward at a constant speed. The sensors logged the damping force experience by the vessel. The speeds and resulting damping forces is presented in the results section.

3.3 Results

The measurements collected by the sensors were saved in text files and imported to MatLab. The measurements fluctuated slightly as seen in the following figure

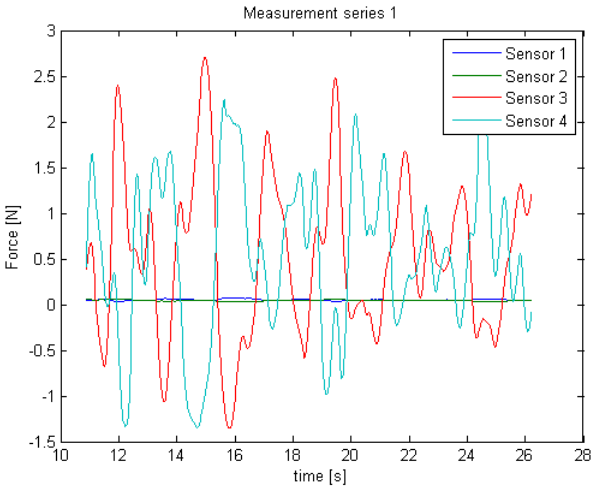

Figure 3.5: Example of measurement from the second bollard pull test

An time period of the graph of special interest had to be identified, and the mean of the 4 sensors were taken over this period. The forces and moments were then calculated according to the setup described in Section 3.2.

3.3.1 Fist bollard pull test

Results from test with different rotational speed

Surge force [N]	Sway force [N]	Yaw moment [Nm]	Left screw rotation speed [rps]
0,4820	-0,0970	0,1126	0,1441
2,1194	0,9987	0,9066	0,4551
3,5825	2,1429	1,6962	0,6286
5,4075	3,2909	2,2101	0,7847
7,8605	5,0741	3,3314	0,9635
10,831	7,1165	4,2172	1,1717
13,7387	8,5472	5,6631	1,3870
16,4131	9,5003	6,6264	1,5747
18,8517	10,9586	6,8543	1,7585
21,2639	12,9428	6,4592	1,9181
24,9150	13,5528	7,3571	2,1272
28,0871	14,5122	8,6200	2,3346

One of the things to notice is the max rotational speed of 2.3 rps. This will be used in the autopilot design.

3.3.2 Second bollard pull test

Results from test with equal rotational speed.

Left screw rotation speed [rps]	Right screw rotation speed [rps]	Resulting surge force [N]
0	0	0
0,1896	0,1875	0,8456
0,4557	0,4910	4,9106
0,5712	0,6371	8,1073
0,7840	0,8136	13,4816
1,1633	1,1713	27,0559
1,3312	1,3343	32,2813
1,5015	1,5258	38,7216
1,6835	1,6861	44,3214
1,7958	1,8630	49,2195
1,9520	1,9927	54,5357

3.3.3 Surge damping test

Carriage speed $[\frac{m}{s}]$	Surge resistance [N]
0	0
0,05	0,0905
0,1	0,3093
0,15	0,6914
0,2	1,2418
0,3	2,7789
0,4	5,2225
0,5	8,1958

3.4 Identifying thrust allocation

In this section we are trying to determine the parameters k_x and k_y introduced in Section 2.5.1. This will be done by using the MatLab Curve Fitting toolbox which gives the parameters to a given equation for a single-input single-output system. The parameters are chosen as the ones that gives the least root mean squared error (RMSE).

$$RMSE = \sqrt{\frac{\sum_{i=1}^{n}(y_i - \bar{y}_i)^2}{v}} \tag{3.1}$$

where y_i is the measured value, $\bar{y}_i$ is the estimated value and v is the number of measured values. The lower the RMSE value, the better the fit.

The first test to identify is the second bollard pull test, with data presented in Section 3.3.2, done with equal rotation on both screws. The reason for doing this first is that it should give the most accurate k_x value, which will then be used to determine the k_y value later.

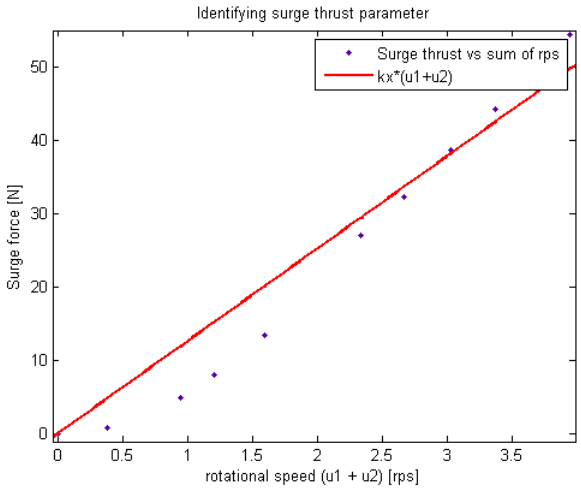

Figure 3.6: Surge thrust with fitted curve

Here we see the the actual and fitted curve. The resulting parameter is $k_x = 12.63$, but with a RMSE of 4.511 which is almost 10% of the maximum value and therefore may be to high. A second degree equation may lead to a better fit for the entire plot, but we want a linear term to describe the thrust. If we look closely at Figure 3.6 it seems to be linear once a certain rotational speed is reached. A second attempt of fitting the graph is then made.

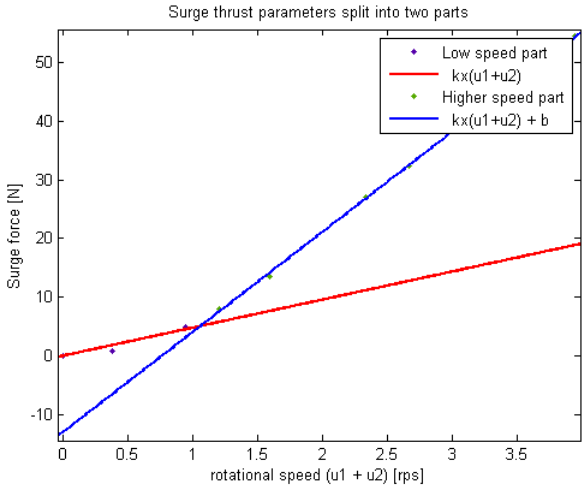

Figure 3.7: Surge thrust split into two parts with fitted curve

The low speed part of this figure gives us $k_x = 4.784$ with a RMSE of 0.7298, which is still a high error compared to the highest surge thrust of $4.91[N]$. The second part however fits much better. The target equation here must be on the form $y = ax + b$ since we can not demand the equation being zero at $u1 + u2 = 0$. The resulting equation is $T_s = 17.07 * (u_1 + u_2) - 13.07$ with a RMSE of 0.4183. The error has been reduced by a factor of ten. However, special attention must be made for the transition between the two fits to prevent any singularities, and the forward speed needs to be monitored to know when to use which parameter. For this reason, it is $k_x = 12.63$ that will be used in this thesis.

When identifying k_y we look at the measurements done in the first bollard pull test, shown in Section 3.3.1. Here we have measurements of surge, sway and yaw forces. As illustrated in Figure 2.6, the moment generated by the vessel is solely depending on the surge force. However the moment generates a measured force in sway which does not have its origin in the rotation screws. In order to identify which part of the measured moment comes from the sway force, we use the k_x value derived above to determine the moment from surge. Subtracting this from the measured moment and dividing the resulting difference by the distance between the center of the vessel and the point of measurement gives us the sway force that generates momentum. As previously stated, the sway force does not generate momentum, so we need to subtract this from the measured sway resulting in the actual sway force generated by the screws.

$$\begin{aligned} M_x &= k_x l(u_1 + u_2) \\ M_y &= M - M_x \\ dY &= \frac{M_y}{b} \\ Y_a &= Y - dY \end{aligned}$$

where M_x and M_y is the part of the moment belonging to measured surge and sway forces. M and Y is the measured yaw moment and sway force. The moment arms l and b is defined in Figure 3.2 and are 0.22 and 0.4 respectively, and dY is the sway force adding to the moment. Y_a is the actual sway force. Plotting this in the MatLab Curve Fit toolbox gives

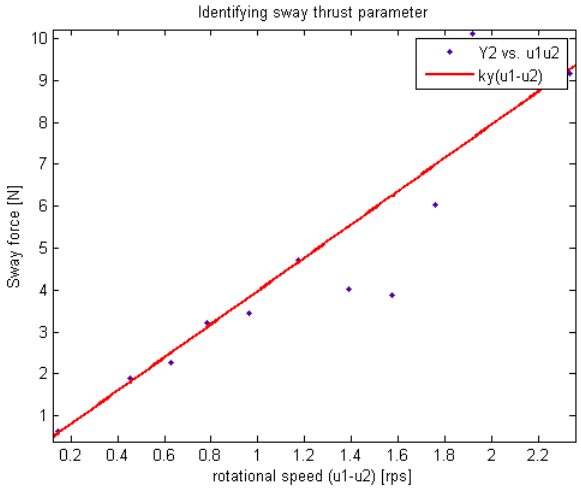

Figure 3.8: Sway force with fitted curve

where $k_y = 3.97$ with a RMSE of 1.26. This is a very high error, but from looking at the figure we see that this error starts after $u_1 - u_2 = u_1 = 1.2[rps]$. We will assume that there are nonlinearities that are unaccounted for.

3.5 Identifying surge damping

The results from the test is shown in the table in Section 3.3.3. As previously stated, yz-symmetry is assumed. This means that the same damping forces are the same, but in the opposite direction, for negative speeds. The resulting damping curve is plotted in the following graph.

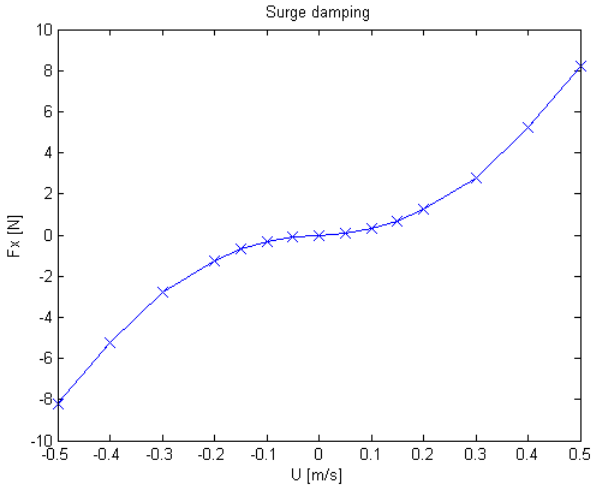

Figure 3.9: Surge damping result

According to section 3.5 in Fossen (2010), the equation for surge speed can be given as

$$(m - X_{\dot{u}}) - X_u u - X_{|u|u}|u|u = \tau_1 \tag{3.2}$$

where m is the mass of the vessel, u is forward speed, $X_{\dot{u}}$ is the added mass, X_u is the linear damping parameter, $X_{|u|u}$ is the non-linear damping parameter and τ_1 is the resulting force in surge. Using the results shown in figure 3.9, we can determine the parameters in this equation. Since the tests were done with constant speed, the derivative part is set equal to zero and is removed. The equation to be identified by the MatLab Curve Fit toolbox is then

$$-X_u u - X_{|u|u}|u|u = \tau_1 \tag{3.3}$$

where u is given by the x-axis of the figure 3.9, and τ_1 is the y-axis of the same figure. The results of the curve fitting were

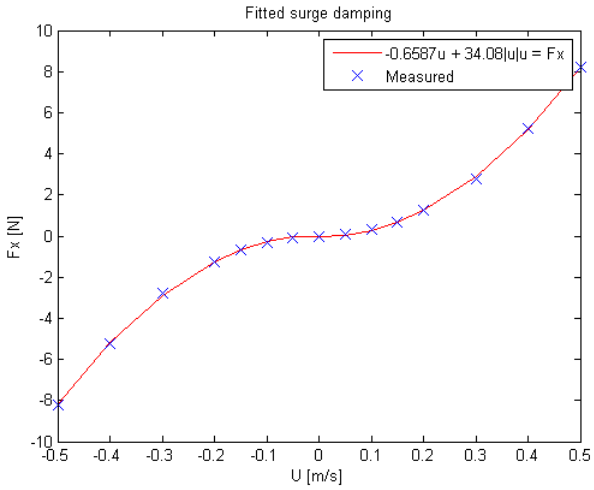

Figure 3.10: Curve fitted surge damping

where it is seen that for $X_u = -0.6587$ and $X_{|u|u} = 34.08$, showing and RMS error of 0.04411. However the damping matrix needs to be positive definite, that is $\mathbf{D} > 0$. This is because the function of the damping matrix is to remove energy from the system. A negative damping matrix will result in the simulated system receiving energy and its states will quickly reach infinity. Because of this, the X_u value determined here can not be used. It will be set as zero from here on. The rest of the parameters in Equation 2.24 needs to be filled in. Based on the surge damping found here, we assume that the damping in sway and yaw are substantially larger, and that the interconnected damping is also quite a bit larger. The assumed values are $Y_{|v|v}|v_r| + Y_{|r|v}|r| = 300$, $Y_{|v|r}|v_r| + Y_{|r|r}|r| = N_{|v|v}|v_r| + N_{|r|v}|r| = 60$ and $N_{|v|r}|v_r| + N_{|r|r}|r| = 200$.

3.6 Resulting model

Using thrust allocation model described in Section 2.5.1 with the values $k_x = 12.63$ and $k_y = 3.97$.

$$\tau_b = TKu = \begin{bmatrix} 1 & 0 & 1 & 0 \\ 0 & 1 & 0 & -1 \\ l_y & 0 & l_y & 0 \end{bmatrix} \begin{bmatrix} 12.63 & 0 \\ 3.97 & 0 \\ 0 & 12.63 \\ 0 & 3.97 \end{bmatrix} \begin{bmatrix} u_1 \\ u_2 \end{bmatrix} \tag{3.4}$$

Using the damping matrix described in Section 2.4.3 with $X_u = 0$ and $X_{|u|u} = 34.08$.

$$\mathbf{D}(\boldsymbol{\nu})\boldsymbol{\nu} = \begin{bmatrix} 0 & 0 & 0 \\ 0 & 0 & 0 \\ 0 & 0 & 0 \end{bmatrix} \boldsymbol{\nu} + \begin{bmatrix} 34.08 & 0 & 0 \\ 0 & 300 & 60 \\ 0 & 60 & 200 \end{bmatrix} |\boldsymbol{\nu}|\boldsymbol{\nu} \tag{3.5}$$

Chapter 4

Joystick control design

4.1 Problem statement

Joystick control is a commonly used method of controlling a marine vessel. In many cases it is a part of a dynamic positioning system where the joystick is used by an operator to set a thrust or a rotation in the direction he or she chooses. For a fully actuated vessel, this means that the operator can have full control over all the DOFs available. The commanded thrust or rotation is given in the NED-frame and have to be transformed into the body-frame equivalent to be able to calculate the correct thruster force and position, if the thrusters are movable. The change from NED to body is presented in Section 2.2 in Fossen (2010) and states

$$\tau_N = R(\psi)\tau_b \tag{4.1}$$

where τ_N is the commanded rotation or thrust in the NED-frame, and τ_b is the same in the body frame. The $R(\psi)$ matrix is discussed in Section 2.1. We then multiply $R^T(\psi)$ on the left side of both sides of the equal sign, and since $RR^T = I$ we get

$$\tau_b = R^T(\psi)\tau_N \tag{4.2}$$

which is then given to the thrust allocation, which will be discussed shortly, to decide the best setup of thrusters to achieve the task.

This is, as stated, for a fully actuated vessel. However, as discussed earlier in this thesis, the OSF is not fully actuated. It can produce thrust, with its two screws, in surge direction and a yaw moment, but no force in sway. At least not simultaneous with surge and yaw. If we look at the thrust allocation equation derived in Section 3.4 we see that this is a 2-by-3 matrix. The only way to transform desired force into screw speed is by inverting this matrix, but since it is not square this can not be done. The only way to do this is by using the pseudo inverse presented in Section 9.7.2 in Fossen (2010), $T^\dagger = T^T(TT^T)^{-1}$. However, the resulting vector is not enough to guarantee a correct movement since the sway force is depending on surge and yaw. This makes the more traditional approach to joystick control described above impossible to implement, and we have to look at alternatives. The seemingly best option is to make a heading autopilot where the desired heading is set by the operator and given to a controller that does the necessary changes in produced thrust in order to reach that heading. The next chapter will describe the

autopilot. Controlling the speed of the vessel is also needed, so a method of doing this with the same joystick would be advantageous for the simplicity of the HMI (Human Machine Interface).

On land, this is different. Without the possibility of changing heading without any surge velocity, control in the NED-frame is impractical. In Section 2.2 the workspace and configuration space of the OSF was presented. Here it was presented that on land, the OSF can control either surge and yaw together or sway alone. Since we should utilize the opportunity of a third controllable direction of motion we need to control the body-fixed velocities. A consideration needed to be made is that it can be confusing for the operator to switch between two frames, but if we put strict limitations on max velocities and accelerations to prevent sudden changes, this should hopefully be a matter of experience.

4.1.1 Equipment used in design

The joystick used in designing the control for this thesis is not very well suited for the task. It is a rather cheap one meant to be used in computer games. It is not made to be left in a position other than the center, and it takes very little force to move it from the center to the edges. This means that it is very hard to keep in a given position, and the only way to make the output stable is by leaning it into an edge. It does however have a one dimensional lever intended for thrust control in aeroplane simulators. This will be utilized as the surge speed control in this thesis, and the joystick itself will be used to give desired heading.

4.2 Thrust allocation on land

On land, the screws work in a different manner. The important factor is the surface the screws operate on, since this will determine the traction they will get. It is assumed that a good grip situation is when the screws can dig into the surface, and use the size of the thread to generate thrust as seen in figure 4.1(a), and not just rely on friction between the thread and the surface as seen in figure 4.1(b).

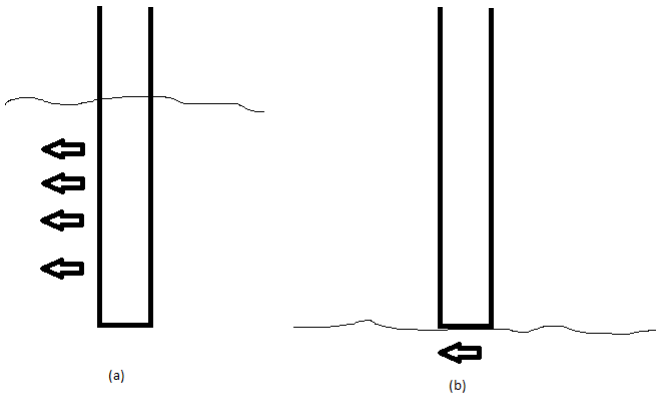

Figure 4.1: Traction situations

When both screws rotate in a positive direction the vehicle will move forward if there is enough grip. Without good traction there is a risk of spinning the screws. Sideways motion will occur when the screws rotate in the opposite direction. As the model used in the MCLab tests were made mainly for operation in water, this has not been tested. It is not known how this will work on the full-scale prototype but preliminary tests done by M-Tech shows that on soft soil sideways motion occurred at very slow speeds. This means that the weight of the vehicle and the traction of the screws are not enough to overpower the shear force generated by the attempted rotation.

The force created by the screws when working on land can not be set up in the same manner as on water. The concept of thrust does not exist on land, only force created by the movers which we normally think of as wheels. On water, as has been discussed, the method of choice is to calculate the force generated by the rotating screws. On land, the velocity of the vehicle is decided by the pitch of the screws in combination with the speed of rotation. Thus, the best method of modelling the movement of the vehicle as a function of the screw velocity, found in this thesis, is by defining equations for each of the DOFs. Because of the different effect the screws have on different types of surface, we assume the surface to be soft enough for the screws to sink in as shown in Figure 4.1(a). This means that the forward speed is defined by the slowest screw. If the other screw is rotating faster than the other on this type of surface, it is assumed here that the fastest screw will not be able to drag the slowest, and thus the difference in rotational speed is shown as a change in heading. For the sideways velocity that has been discussed it is assumed that the fastest screw can pull the slower, and thus the sideways motion will be the mean rotational speed of the two screws times the diameter of the screws. The resulting equations are

$$\boldsymbol{\nu} =$$

$$u = pitch\frac{u_1 + u_2}{2} \tag{4.3}$$

$$v = diameter\frac{u_1 + u_2}{2} \tag{4.4}$$

$$r = pitch(u_1 - u_2) \tag{4.5}$$

where u_1 and u_2 is the rotational speed of the screws. Pitch and diameter is 0.35 and 0.465 respectively. Because of the max and min values it is not possible to transform these equation into a matrix form, and the speeds have to be calculated one by one. Since no experiments have been made on movement on land, neither acceleration nor top speed is known. The only parameter known is max rotational speed in water which is $/2.3\frac{rot}{s}$. However, with no knowledge of traction or efficiency, and the fact that operation on land, at least for the full-scale vessel, means a possibility of close proximity to humans, the max rotational speed will have to be severely limited on land.

Because of this, the velocity on land should be severely limited in order to avoid loosing traction. A max forward speed of $2\frac{m}{s}$ and max sideways speed of $1\frac{m}{s}$ is set for this thesis. This is not based on measurements but on the need to set a speed on which to work from. Testing of the full-scale OSF will have to be done in order to determine the best suited max speed.

The transition between forward and sideways movement needs to be handled carefully. The model developed for this thesis makes sideways movement impossible unless the operator presses and holds a specific button on the joystick.

4.3 Joystick input

The input from the joystick is received by the computer as x and y coordinates, ranging from $[-1, 1]$.

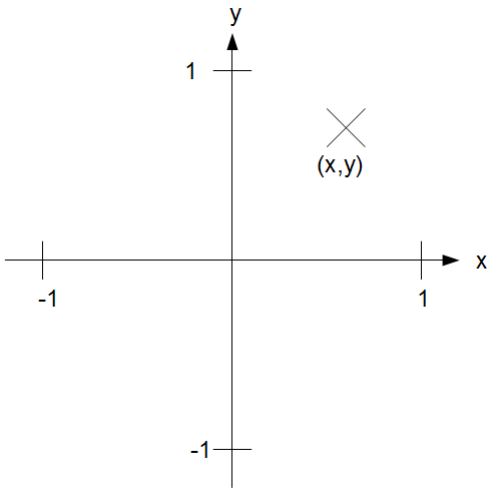

Figure 4.2: Joystick

The desired heading is translated by using these x and y coordinates using the atan2 function. This is a variation of the normal arctangent function with an increased range. A normal arctangent function is defined between $(-\frac{\pi}{2})$ whereas atan2 is defined between $(-\pi, pi]$.

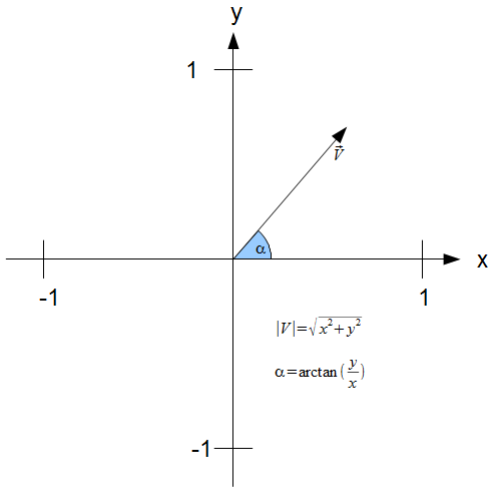

Figure 4.3: Joystick Vector

This angle is then sent through to either the controller or to the vessel dynamics to be used to define the movement of the vessel.

4.4 Output shaping

When the joystick input is changed, the model is supposed to follow. If the change is very fast, the model can not follow since it is limited by physical attributes.

4.4.1 Heading

Using equation 7.22 in Fossen (2010)

$$\ddot{\boldsymbol{\psi}}_d + 2\boldsymbol{\Delta}\boldsymbol{\Omega}\dot{\boldsymbol{\psi}}_d + \boldsymbol{\Omega}^2\boldsymbol{\psi}_d = \boldsymbol{\Omega}^2\mathbf{r}^b \tag{4.6}$$

where $\boldsymbol{\psi}_d$ is the desired heading. The matrices $\boldsymbol{\Omega}$ and $\boldsymbol{\Delta}$ are positive definite diagonal matrices that can be interpreted as natural frequencies and relative damping ratio respectively, and $\mathbf{r}$ is the input that in this case is the heading set by the user. This is a second order model, and thus creates a smooth reference signal for up to a double derivative of ψ_d. This is needed for the controller which will be discussed later.

The parameters are chosen as $\boldsymbol{\Omega} = 0.5$ and $\boldsymbol{\Delta} = 1$.

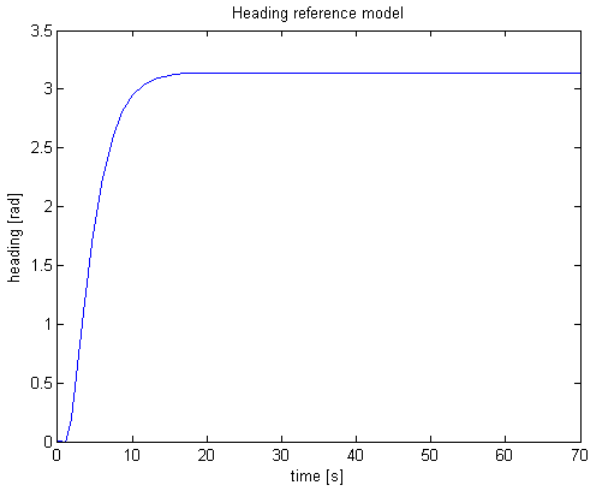

Figure 4.4: Heading reference model performance

They are chosen arbitrarily for their performance. Because of the agility of the vessel, the turn rate has been set quite fast as can be seen in Figure 4.4

4.4.2 Mechanical dynamics

In reality, whenever the rotational speeds of the screws are changed, the inertia of the screws make the change happen over time. This delay is usually defined as a function of

torque and the screws moment of inertia. This delay should be on the form depicted in Figure 4.4, albeit quite a bit faster, since it the screws should have a smooth acceleration curve. However, when this was implemented the system started to oscillate violently, and the plots showing the screws rotational speed showed signs of aliasing. The source of this was not identified. Therefore, the mechanical dynamics had to be simulated on the form of a low-pass filter as described in Fossen (2010).

$$\omega_n r = \dot{\nu}_d + \omega_n \nu. \tag{4.7}$$

A similar equation is used in Section 6.6 in Sørensen (2006) for modelling a propeller shaft, however that model is based on knowledge of produced torque and energy lost to friction. In this thesis the torque generated by the motors are unknown, so the low-pass filter is based on assumptions which again is based on observations done during testing. These observations show that the screws go from zero to max rotational speed and back again to zero very fast, so the filter should be tuned to reach the target velocity fast. For this thesis, $\omega_n = 4$ is used. This reaches the target speed in two seconds.

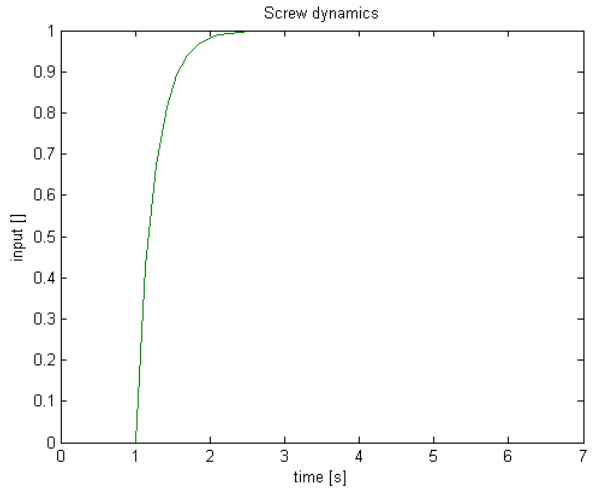

Figure 4.5: Dynamics of thruster

4.5 Open-loop control on land

To model the motion on land we will be using the equation derived in Section 2.3. This holds for motion on both land and water. However some alterations must be made. The $\boldsymbol{\tau}_{RB}$ is now only made up of the forces created by the screws, since no hydrodynamic forces or environmental forces apply on land.

The joystick sets a vector that determines the movement of the vessel in the body frame. The slide, denoted S from here on, defines the length of the vector and the joystick defines the angle. As seen in Figure 4.2 and Figure 4.3 the joystick provides x and y coordinates which describe the angle. This vector sets the speed of the screws according to the following equations:

$$u_1 = Sx(0.9 + 0.05y) \tag{4.8}$$
$$u_2 = Sx(0.9 - 0.05y). \tag{4.9}$$

Here we see that when the joystick is pointing straight ahead and the slide is placed fully forward, i.e. $S = 1$, $x = 1$ and $y = 0$, the rotational speed of both screws are set as 0.9. If the $x = 0$ we see that the rotational speed is set to zero. This is because, as previously discussed, it is suspected that it is impossible to do on-the-spot rotation on land. The constants 0.9 and 0.05 is arbitrarily set to reflect the assumed dynamics. The screws rotation is translated into body-fixed vehicle speed through Equation 4.3, which is then sent to a filter. This filter is meant to combine the need for a smooth output with the presence of mechanical dynamics like the screws needing an amount of time to reach the target velocity. This will be discussed in more detail in the next chapter. These velocities are then converted to forces using a gain set as $[201010]^T$. This is arbitrary since no testing has been done to identify the forces generated on land. The values are chosen purely for the reason that they work. The forces are then fed into the rigid body dynamics, which gives a body-fixed velocity. This is then sent through a rotation matrix in order to plot the North and East coordinates of the vehicle.

4.5.1 Simulation results

The following plots show the performance of the open-loop control. Please note that the velocities are not correct. The parameters in this model has, as has been stated, chosen on the basis that they provide results that helped to verify the model structure. In the first figure we see the movement of the vessel when commanded to move in a zigzag pattern. The second figure is the velocities of that movement.

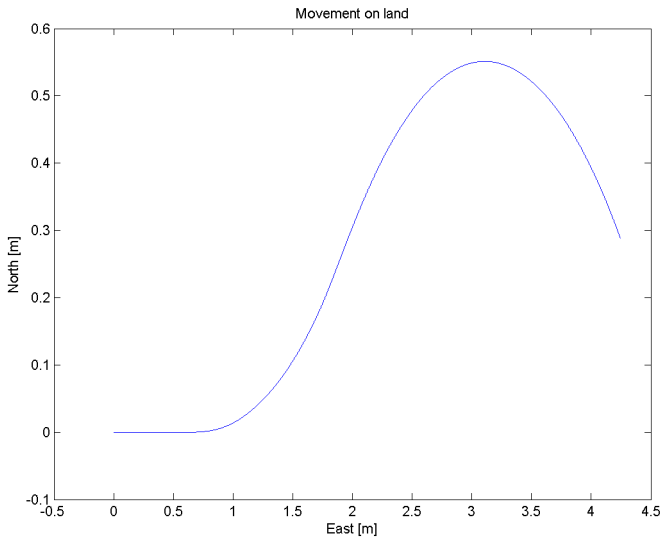

Figure 4.6: Movement on land

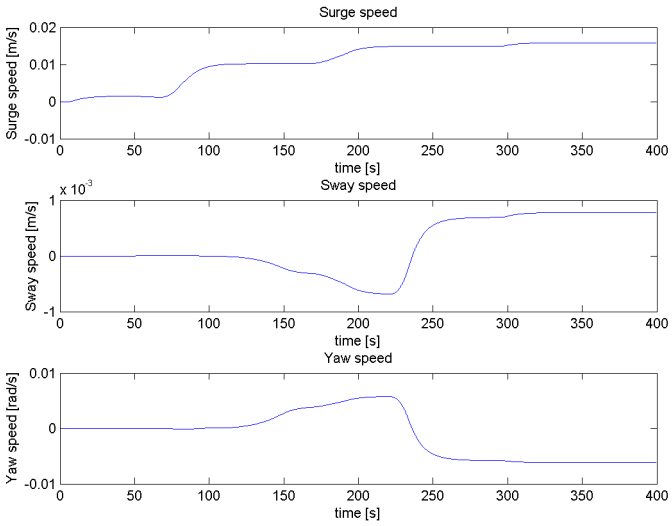

Figure 4.7: velocities on land

The next figure shows the sideways movement function. Here, the vessel is first set to move straight ahead. When almost 150 seconds have passed, the command to switch to sideways motion is given.

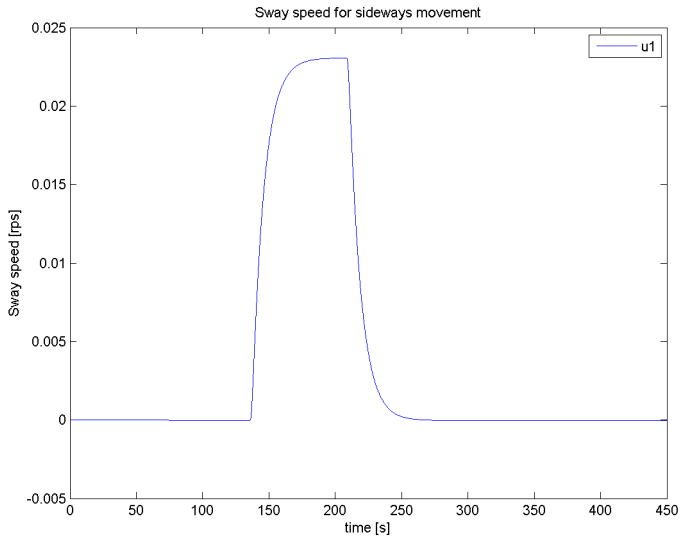

Figure 4.8: Sideways speed

4.6 Maneuverability and Open-loop stability

In order to find out what to expect from the model, a variety of tests have been devised to determine the maneuverability and stability. Essentially, maneuverability means how the vessel responds to produced thrust. Stability, or open-loop stability as it is called, means how the vessel responds to disturbances, usually in yaw. Good stability comes

from sacrificing maneuverability and vice versa. More on the maneuverability of vessels can be found in Berg (2009). The test done to determine the maneuverability of the OSF model will be the turning circle test. When discussing stability, there are two definitions. Straight-line and course stability. Both will be presented in this chapter.

4.6.1 Open-loop stability

Defined in Fossen (2010) as the ability of a vessel to return to an equilibrium after a disturbance without any action corrective action of the actuators. This can be divided into two different definitions. Straight-line and directional stability.

Straight-line stability	If an uncontrolled vessel moving in a straight line and continues to move in a straight line after being influenced by a disturbance in yaw, that vessel is considered straight-line stable. Note that in this case the course of the vessel has changed.
Directional stability	Much stronger requirement than straight-line stability. Here, if the vessel moving in a straight line is disturbed in yaw and returns to the same course as prior to the disturbance on its own accord, i.e. without controller action, the vessel is said to be directional stable.

When testing the stability of the model, the only input was the screws rotational velocity. This was transformed into forces, and the mathematical model calculated the movement. Those movements show instability for a disturbance in yaw. This disturbance has been modeled as a spike in one of the screws rotational velocity, and results in an undamped yaw moment i.e. a constant turn rate, as shown in the figures below.

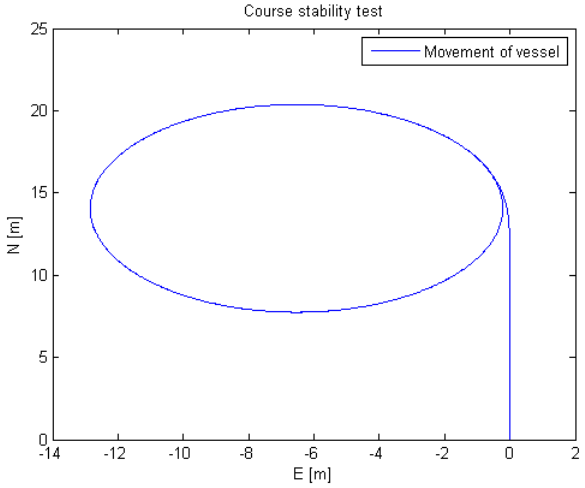

Figure 4.9: Course stability test

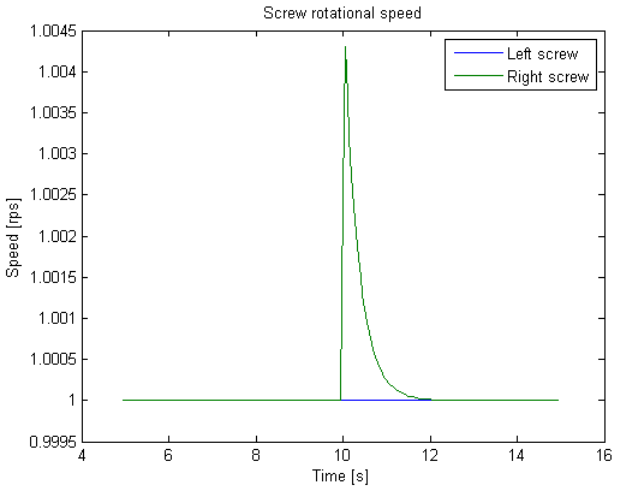

Figure 4.10: Screw rotational speed in course stability test

4.6.2 Turning circle test

When performing a turning circle test it is usual to model the vessels rotational inertia using the Nomoto model presented in Berg (2009). This is done for cases where all we have to go on is the vessels measured performance. For this case, since we do not have any measurements on the OSF model doing any maneuvers, we use the developed mathematical model to get these measurements. So going through the Nomoto model is unnecessarily complicated since we have perfect knowledge of the parameters used to obtain the measurements. The test was done by taking the model used for stability testing, and giving one of the screws a series of rising velocities starting at 0 rps and ending at 1 rps. The other screw was kept at 1 rps. Measurements of the vessels surge, sway and yaw speeds, as well as the thrust the screws produced, were taken well into the test when the movement was well underway. The resulting radii of the circles were

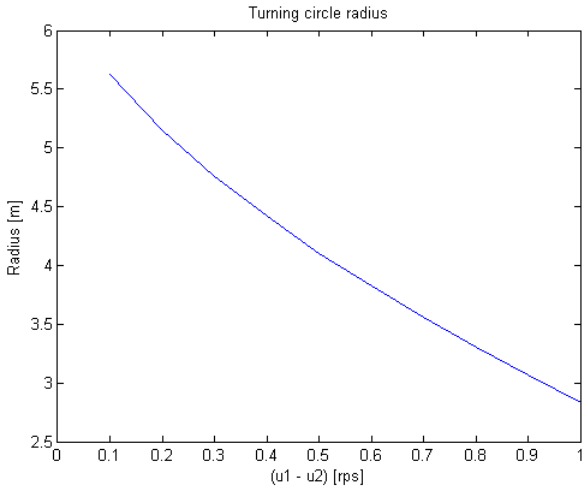

Figure 4.11: Turning circle test radius

The curve showing the radius should go to a much higher value when the difference in

screw rotation went to zero, but as has been seen in Section 4.6 the vessel is unstable. Even a slight disturbance in yaw created a circle movement with radius around 6m. It is therefore no surprise that the radius seem to point towards 6m as the difference in screw rotation goes to zero. However, if we design a non-dimensional way of measuring the maneuverability, call it yaw factor, we see that it does indeed climb quickly when $(u_1 - u_2) \rightarrow 0$. The non-dimensional parameter is calculated like this.

$$\frac{yawrate[\frac{rad}{s}]}{angle[rad]} Time[s] = [] \tag{4.10}$$

where the angle can be thought of as a pseudo rudder angle, illustrated below, and time is the time used to do an entire circle.

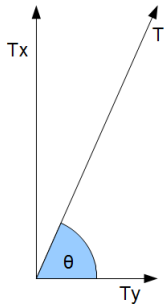

Figure 4.12: Pseudo rudder angle

Here, Tx is the surge thrust, Ty is the sway thrust and T is the resulting thrust. Θ is the angle between the two, and is the pseudo rudder angle. Using this angle in the non-dimensional equation gives

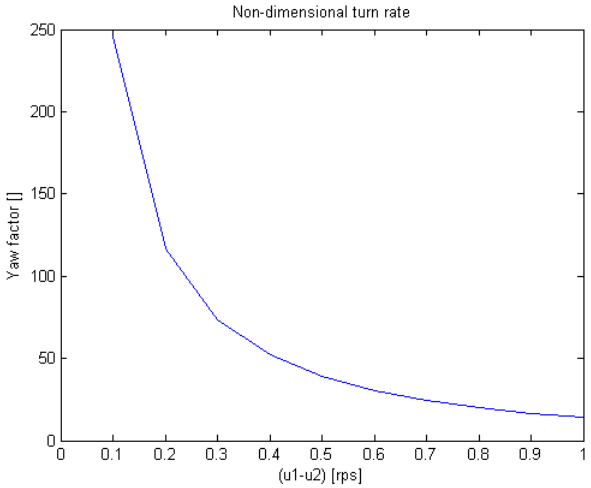

Figure 4.13: Non dimensional turn rate

When testing the model for opposite screw speeds, $u = [1 - 1]^T$, nothing else than a commanded yaw moment were given to the model, and the response should be that the vessel turned around its own heave-axis. What was observed however was the presence of both surge and sway speeds. I can not explain why these appear, but the result is that the model can not turn around its own axis. The velocities are small, around -0.07 $\frac{m}{s}$ in both surge and sway, but they should not be there.

4.6.3 Sideways movement

As introduced in Section 2.5.1, moving the vessel in sway should be possible if we sacrifice the control of surge and yaw. This has been attempted by using a sine input for one of the screws, while the other is kept still. The results show signs of sideways motion but all the velocities oscillate quite heavily. This is mainly because of the sine input given with an amplitude of 0.2 and a frequency of 2, but also due to unmodeled dynamics.

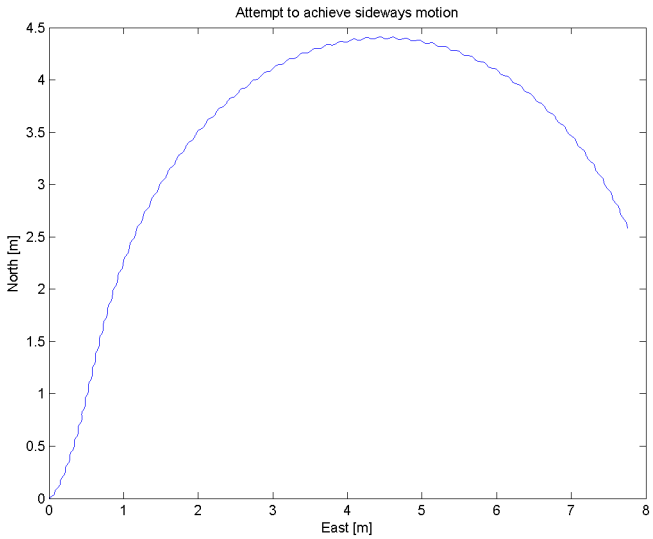

Figure 4.14: Test to achieve sideways movement

Recall here the vessel starts out pointing east.

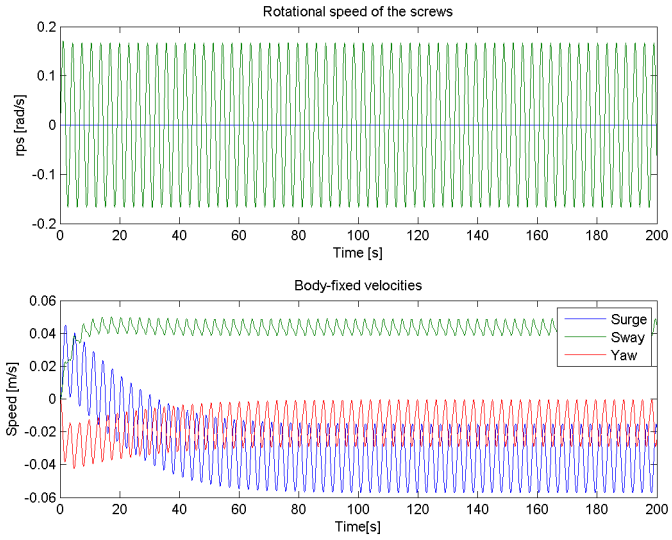

Figure 4.15: Performance during sideways movement

The velocities show that the sway speed is indeed the highest, but the other velocities are to big for it to be possible to use this maneuver in practice. When discussing hydro-

dynamic damping it was mentioned that no measurements had been done in sway. It is likely that it is the assumed values in the damping matrix that causes these effects, but because of this it is hard to say if a sideways motion alone is possible.

Chapter 5

Autopilot control design

5.1 Problem statement

As discussed in Chapter 4 we cannot use the joystick to define forces in the body-fixed frame in an open-loop design, but we can use the thruster slide to control surge speed. The joystick will be used to define a desired heading for a closed-loop autopilot control. Two controllers are tried in this thesis. An Integrator backstepping controller and a PID controller. We will look at controller performance and stability for both, and also look at the PID performance with modeled environmental forces.

5.2 Integrator backstepping control

The Integrator backstepping controller is a method of control that utilizes the "good" parts of a system. If for instance the vessel in question is course stable, as discussed in Section 4.6, the controller can make use of this. In the case of the OSF model, there are no good parts for the controller to utilize, and the resulting control law becomes in effect a PID controller which is why a normal PID controller is developed later.

$$\dot{\psi} = r \tag{5.1}$$

$$(I_z - A_{66})\dot{r} + C_{66}r + D_{66}r = \tau_\psi = lk_x(U_1 - U_2)$$

$$M\dot{r} + (C + D)r = \tau_\psi = lk_x(U_1 - U_2) \tag{5.2}$$

where the heading, ψ, is the parameter to be controlled. Input from the joystick is set as desired heading and is denoted ψ_d. Output is the difference in screw-velocity needed to reach that desired heading. The following controller is based on an example in section 9.5.3 in Fossen (2010), which explains a backstepping controller to a single-input single-output system. The example is for a nonlinear control with a nonlinear part to the stabilizing function. This is omitted from the following. First we define the heading error as $e = \psi - \psi_d$, and thus

$$\begin{aligned} z_1 &= e \\ \dot{e} &= \dot{\psi} - \dot{\psi_d} = r - \dot{\psi_d} \\ \dot{z_1} &= \dot{e} \end{aligned} \tag{5.3}$$

where z_1 is a new state variable. We then use r as a virtual control and define it as

$$r = \alpha_1 + z_2 \tag{5.4}$$

where z_2 is another new state variable. We then combine Equation 5.3 and 5.4 to get

$$\dot{z_1} = \alpha_1 + z_2 - \dot{\psi}_d \tag{5.5}$$

where α_1 is a stabilizing function that we set as

$$\alpha_1 = \dot{\psi}_d - k_1 z_1 \tag{5.6}$$

where $k_1 > 0$ is an arbitrary feedback gain that can be tuned to achieve the desired error dynamics, which will be discussed later. Using this, we get

$$\dot{z}_1 = -k_1 z_1 + z_2. \tag{5.7}$$

We then set a candidate Lyapunov function, CLF, that will result in the system loosing energy.

$$V_1 = \frac{1}{2} z_1^2 \tag{5.8}$$

$$\dot{V_1} = z_1 \dot{z_1} \tag{5.9}$$

$$= -k_1 z_1^2 + z_1 z_2. \tag{5.10}$$

Now we look at the z_2 variable. Combining Equation 5.2 with 5.2 we get

$$M\dot{z_2} = M\dot{r} - M\dot{\alpha}_1 \tag{5.11}$$

$$= \tau_\psi - (C + D)r - M\dot{\alpha}_1. \tag{5.12}$$

We then choose a second CLF as

$$V_2 = V_1 + \frac{1}{2} M z_2^2 \tag{5.13}$$

$$\dot{V_2} = \dot{V_1} + M z_2 \dot{z_2} \tag{5.14}$$

$$= -k_1 z_1^2 + z_1 z_2 + z_2[\tau_\psi - (C + D)r - M\dot{\alpha}_1]. \tag{5.15}$$

Since the difference between the velocity of the two screws is the factor we want to determine, we use $\tau_\psi = l k_x (U_1 - U_2)$ to define a control-law. This law is determined so that $\dot{V_2}$ is negative for all values of z. We can then set τ as

$$\tau_\psi = M\dot{\alpha}_1 + (C + D)r - z_1 - k_2 z_2 \tag{5.16}$$

where k_2 is the same as k_1. This is then the resulting control law that will be used when designing the autopilot. Testing shows that

k_1	8
k_2	4

gives good results, as will be shown the section on simulation results.

5.2.1 Stability

To determine if Equation 5.16 results in a stable system, we look at the resulting systems error dynamics. This is constructed from the state variables z_1 and z_2:

$$\begin{bmatrix} 1 & 0 \\ 0 & m \end{bmatrix} = - \begin{bmatrix} k_1 z_1 & 0 \\ 0 & k_2 z_2 \end{bmatrix} \begin{bmatrix} z_1 \\ z_2 \end{bmatrix} + \begin{bmatrix} 0 & 1 \\ -1 & 0 \end{bmatrix} \begin{bmatrix} z_1 \\ z_2 \end{bmatrix} \tag{5.17}$$

which can also be written as

$$\mathbf{M}\dot{\mathbf{z}} - \mathbf{K}(\mathbf{z})\mathbf{z} + \mathbf{S}\mathbf{z}. \tag{5.18}$$

This is then Global Exponentially Stable (GES). This can be seen by inserting the control law in Equation 5.16 into $V_2(\mathbf{z} = \frac{1}{2}\mathbf{z}^T\mathbf{M}\mathbf{z}$ which then becomes $\dot{V}_2(\mathbf{z} = -\mathbf{z}^T\mathbf{K}\mathbf{z}$ since $\mathbf{z}^T\mathbf{S}\mathbf{z} = 0$. This shows

$$\dot{V}_2 = -k_1 z_1^2 - k_2 z_2^2 \tag{5.19}$$

which is negative for all values of z, meaning that the chosen control law will reduce the total energy of the system, i.e. reduce the error.

5.3 PID controller

The PID controller is the most used feedback controller in the industry to day. This is because it is relatively simple to get it to converge to zero.

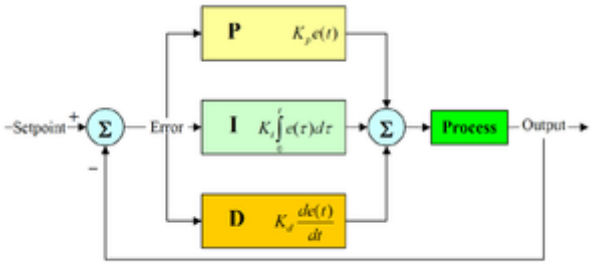

Figure 5.1: PID controller diagram, courtesy of http://en.wikipedia.org/wiki/PID_controller

This figure shows how the controller works. The difference between the desired and actual value is defined as the error, which is then sent through the controller to produce an updated actual value. With positive K_p, K_d and K_i values the error converges to zero. One of the problems with this controller is the phase right after the desired value have been changed, where the sudden increase in error may result in oscillating output. This is normally counteracted by introducing a feed forward term which can be explained as a PD controller using the derivative and double derivative of the desired values as error. These derivatives will be zero when the desired value is left unchanged, but helps the controller reaching the desired value faster.

$$\begin{aligned} \tau_N &= \tau_{ff} - \tau_{PID} \\ \tau_N &= \underbrace{I_z\left(\dot{r}_d + \frac{1}{T} r_d\right)}_{\text{Feed Forward}} - \underbrace{K_p e + K_d \dot{e} + K_i \int_0^t e(\tau) d\tau}_{\text{PID}} \end{aligned} \tag{5.20}$$

where e is the difference between actual and desired heading and r_d is the rate of change in desired heading.

Manual tuning shows that the following K_p, K_d and K_i values gives good performance.

K_p	5
K_d	50
K_i	1.5

5.4 PID controller with bias

Environmental forces are normally considered to be slowly varying and Gaussian distributed, where the mean value of the distribution is the mean value of the forces. Since these forces are slowly varying, it is for modelling purposes a valid assumption to give them a fixed value.

Relative velocity is defined as the difference between the body-fixed velocity of the vessel and the velocity of the current as seen by the vessel.

$$\begin{aligned} \boldsymbol{\nu}_r &= \boldsymbol{\nu} - \boldsymbol{\nu}_c \\ \boldsymbol{\nu}_r &= \boldsymbol{\nu} - \mathbf{R}^T(\psi)\dot{\boldsymbol{\eta}}_c. \end{aligned} \tag{5.21}$$

This can be illustrated as

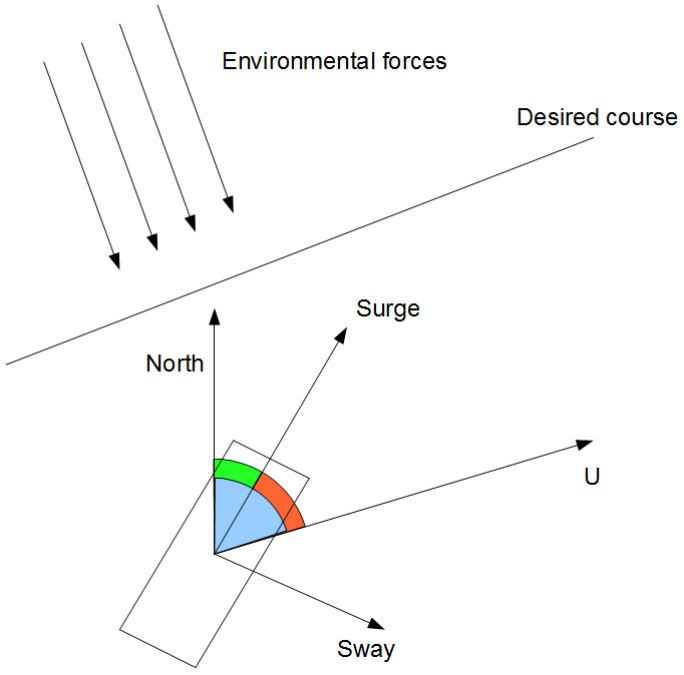

Figure 5.2: Environmental forces

where U is $\boldsymbol{\nu}_r$, the blue angle is the course, the green angle is the heading of the vessel and the red angle is the difference between the two. The following figure shows the heading without bias, course with bias and the difference. The current was set as $\boldsymbol{\nu}_c = [0, -0.2, 0]^T$.

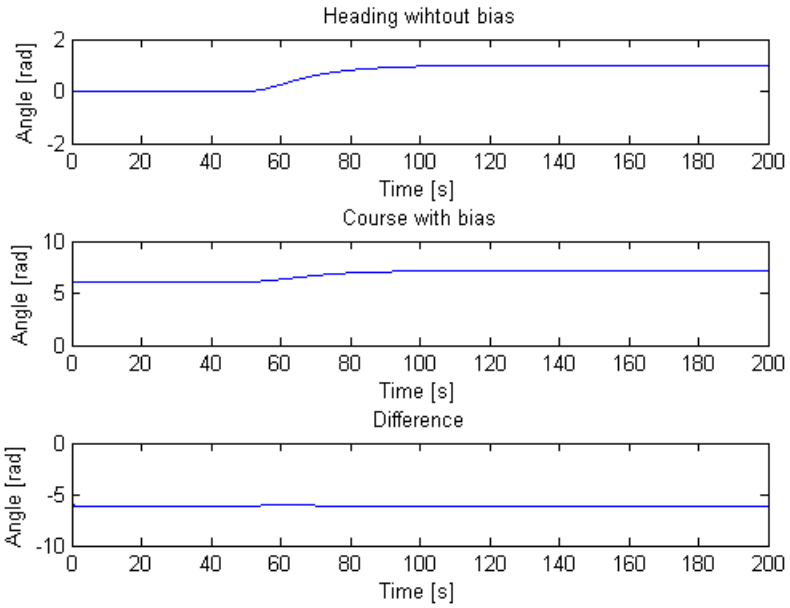

Figure 5.3: Offset caused by current

To control the system with the bias included, control theory tells us that we need an integrator term in our control law to counter the steady state offset that occurs with bias. A method of counteracting the offset shown in Figure 5.3 is given in Section 10.3.2 in Fossen (2011) where it is argued that if you have measurements of the heading and sway speed of the vessel when effected by an environmental force, you can find the desired heading to offset this sway speed by

$$e_\psi = \psi - \psi_d \tag{5.22}$$
$$= \psi - \chi_d + \beta. \tag{5.23}$$

Here, e_ψ is the error heading, χ_d is the desired course , ψ and ψ_d is the vessels heading and desired heading respectively and β is the offset angle introduced by the current. Please note that desired heading and desired course is not the same in this case. Desired heading is the direction the bow of the vessel is pointing while the course is the direction the vessel is actually moving. Because $\psi_d = \chi_d - \beta$, the β angle is used in this version of the PID controller to change the desired heading coming from the joystick. When trying to overcome a bias, it is the integrator term in the PID controller that does the best job. Integrating the error means in reality to sum up the error for each time step, and regulating the system accordingly. If the error does not disappear, the integrator term will keep growing either until it does disappear or the integrators attempt to lessen the error overpowers the other terms. This is called integrator wind-up. It will not be discussed further in this thesis, but is something one needs to be mindful of when designing any system with a possibility for a steady state offset.

5.5 Simulation results

The simulation was done with the force in surge direction set at a constant 50N. The heading starts at zero, but after 50 seconds changes to 1rad using a step function.

5.5.1 Backstepping controller

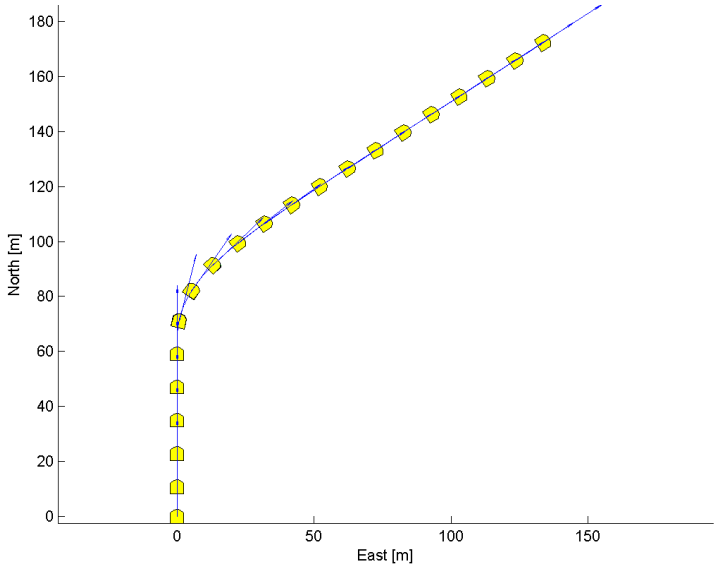

Figure 5.4: Movement of vessel with backstepping controller

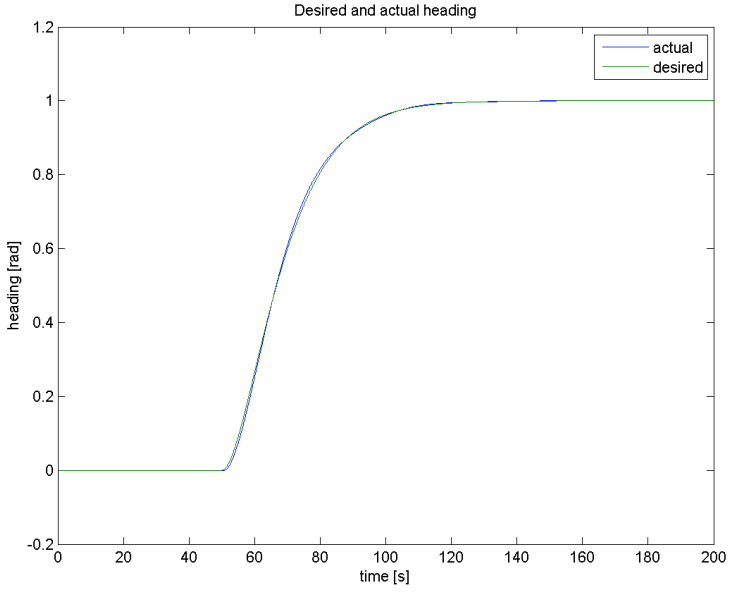

Figure 5.5: Desired heading and actual heading for backstepping controller

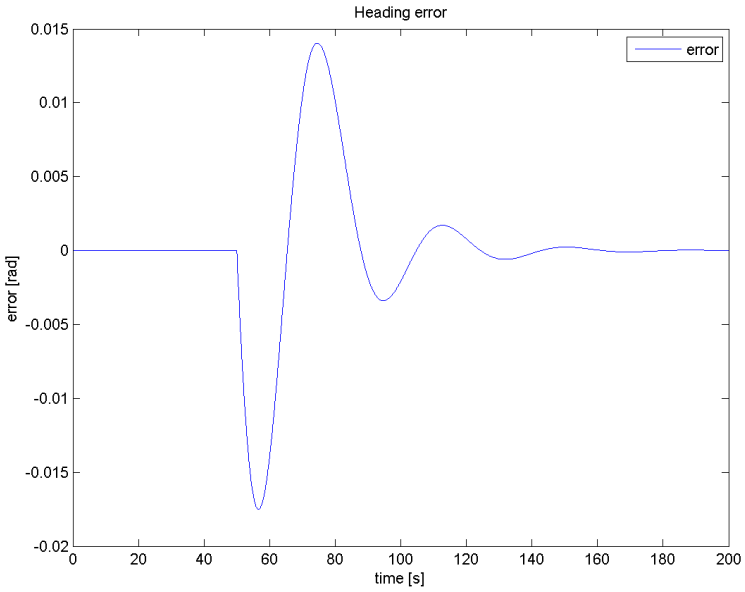

Figure 5.6: Heading error for backstepping controller

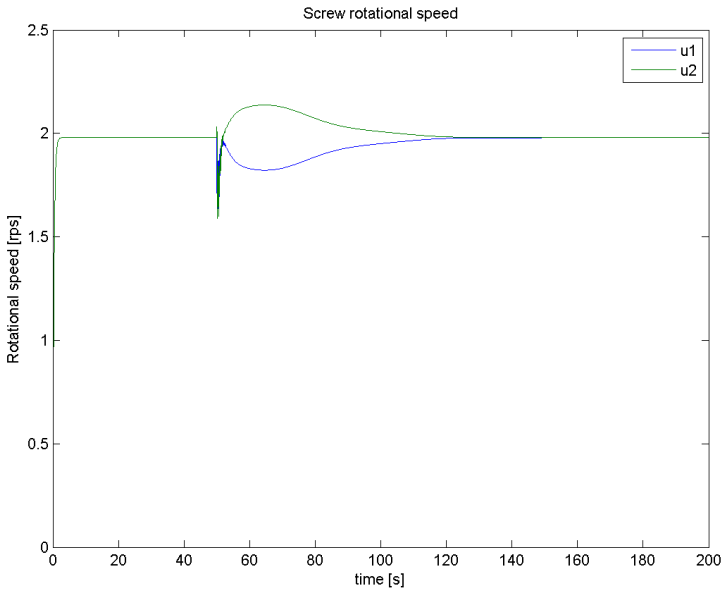

Figure 5.7: Rotational speed of screws with backstepping controller

From these plots we see that the backstepping controller performs very well. There is hardly any heading error, and the rotational velocity of the screws seems sensible except right after the change in heading was given. There seems to be some oscillation before it settles into the correct rps. The source of this may be the incorrectly modeled screw dynamics discussed in Section 4.4.2.

5.5.2 PID controller

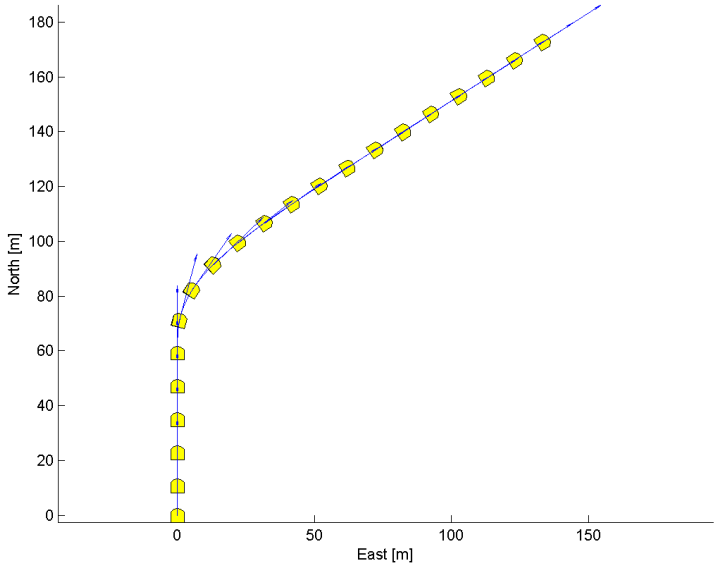

Figure 5.8: Movement of vessel with PID controller

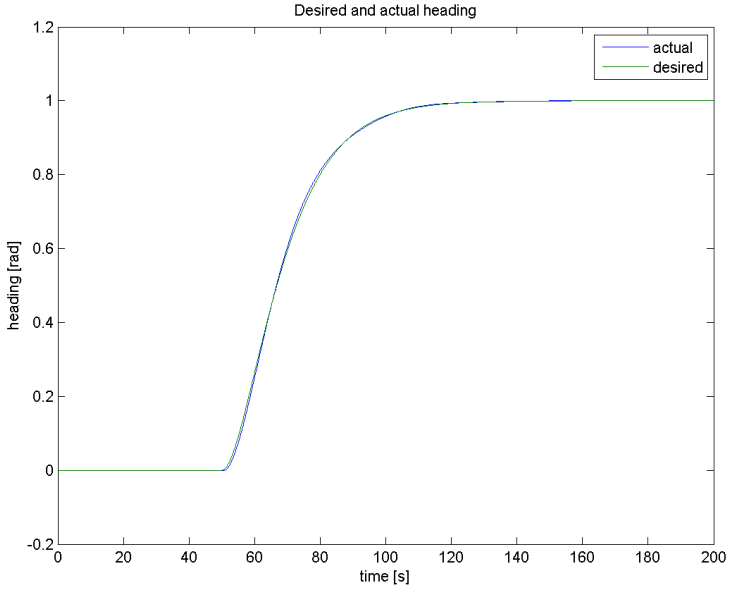

Figure 5.9: Desired heading and actual heading for PID controller

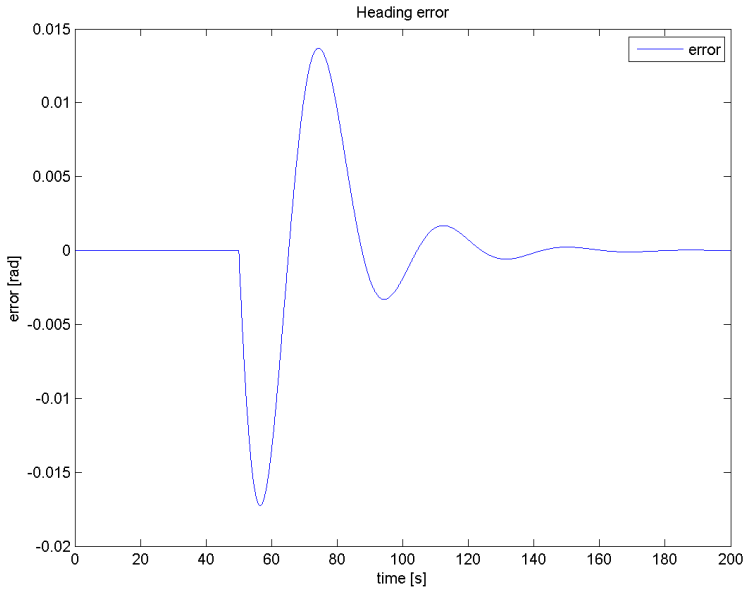

Figure 5.10: Heading error for PID controller

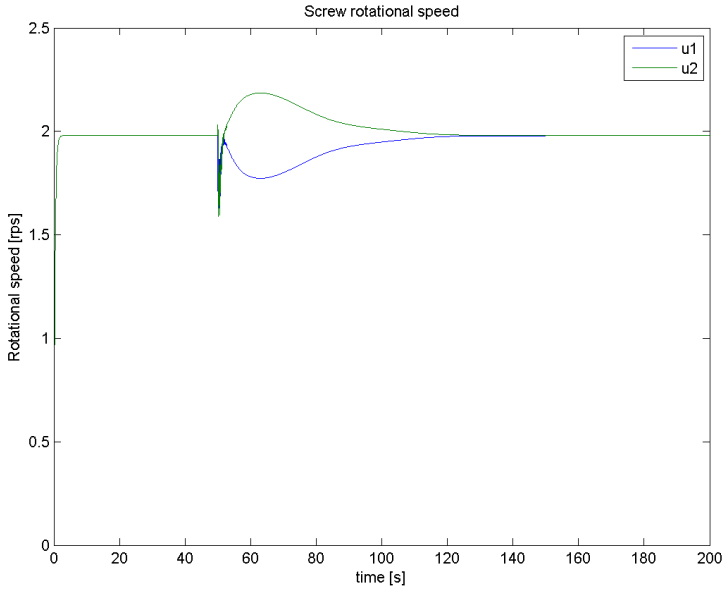

Figure 5.11: Rotational speed of screws with PID controller

The PID controller seem to work much like the backstepping controller. This should mean that the mathematical model developed is, if not accurate, then correctly set up.

5.5.3 PID controller with bias

Current set to be $v_c = [0 - 0.2]^T$

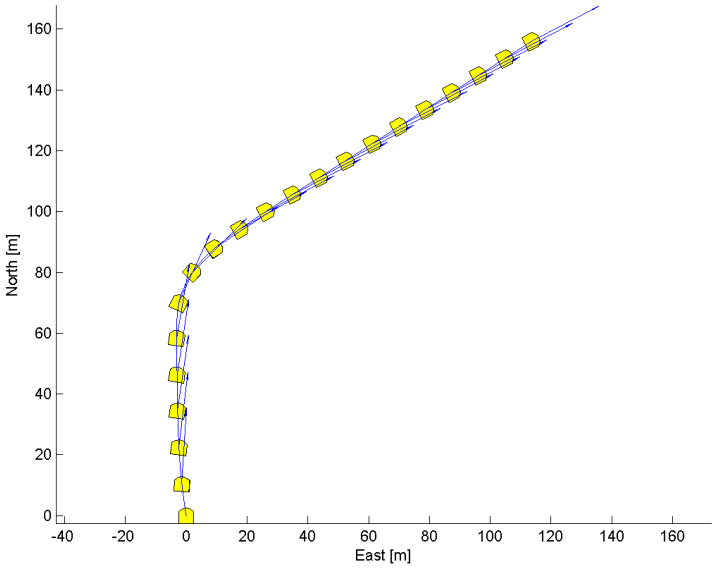

Figure 5.12: Movement of vessel with PID controller and bias

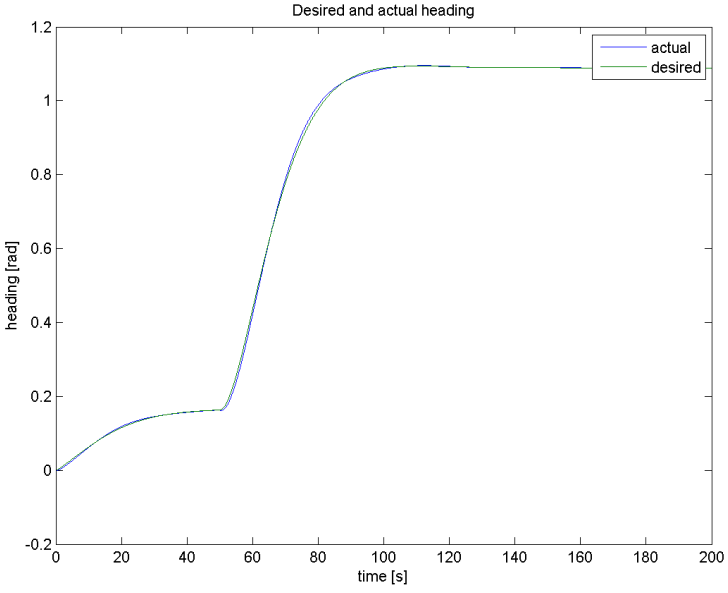

Figure 5.13: Desired heading and actual heading for PID controller and bias

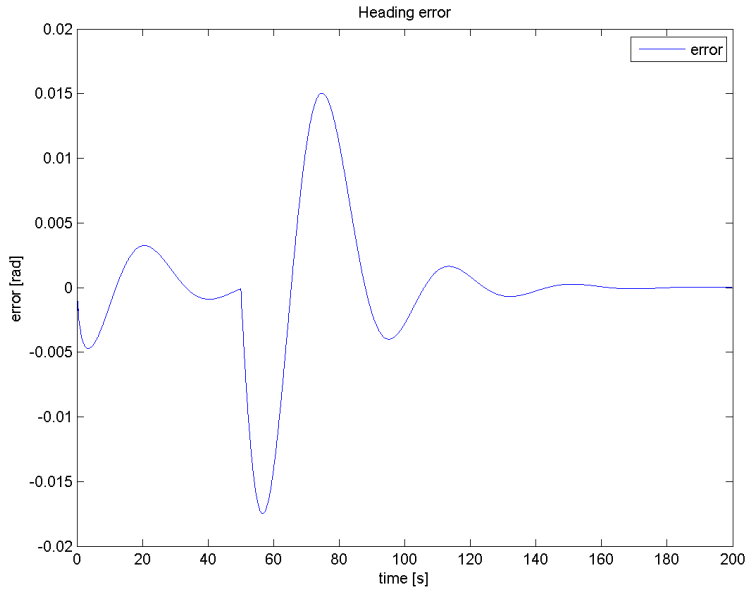

Figure 5.14: Heading error for PID controller and bias

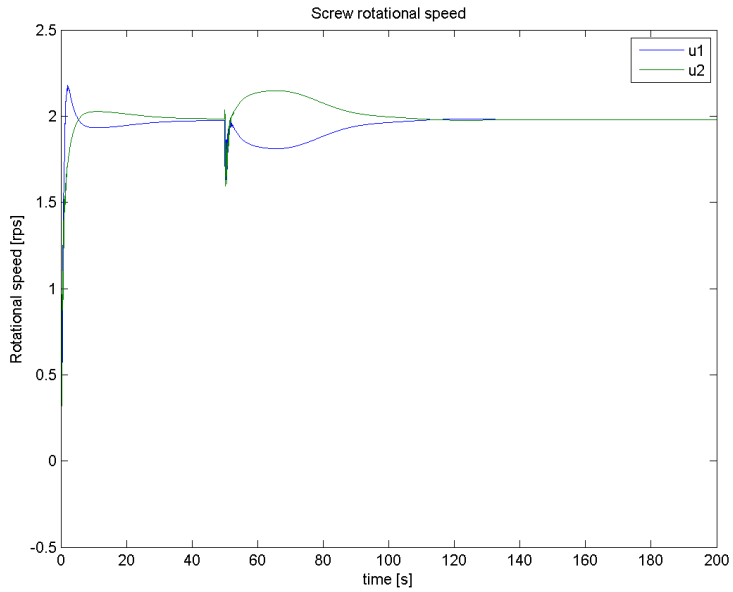

Figure 5.15: Rotational speed of screws with PID controller and bias

The interesting plots appear when we add a current. Here we see the controller struggling a bit more to converge, but being quite accurate non the less. It is possible that special tuning would help in this, but the same gains are used here as in the PID controller without bias. This is done to see the difference in performance, rather than finding the optimal gains for both. We see that the desired heading overshoots the target of 1rad, but this is to be expected since that is the heading the vessel needs to have to keep a course of 1rad in the specified current.

Chapter 6

Transition between water and land

Since the OSF is meant to operate on both land and water, we need to look into how it moves between these two elements. A key part in this is for the vessel to know what kind of surface it is operating. The full scale vessel is equipped with a mechanical torque sensor that lowers the screws rotational velocity whenever it senses an increase in torque. An increase in torque would be felt when the screws rotate on something more solid than water. It could be possible that this would work as a switch for the control system for the full scale vessel. However, since no measurement of the torque developed by the model vessel has been done, it is not known if it is possible to do the same thing here although this is for future work. What is necessary to point out though is the need to slow down before making landfall with the model. It may be obvious, but it is easy to forget when one develops these models mostly on computers.

6.1 Combining land and water models

6.1.1 Combining the two models

The difficulty in modelling this system was changing the initial conditions of the integrators. If the operator takes control of the vessel when it is in a position land, the system defines that position as the origin of the NE-frame. When the vessel moves, it shows the position in relation to this point. When the vessel moves into the water, the position changes. When the operator gives the signal that the water model is to be used, the integrators in this model need to know the current position and velocity and start integrating from there. The first attempts to solve this resulted in algebraic loops in Simulink. Algebraic loops are described in the Simulink help file as a case when a block output depends on the value of an input port, i.e. $y = x + y$. The algebraic loop problem was solved using the GOTO and FROM blocks in Simulink, which is implemented just for cases like this. They provide a connection between two systems by continuously updating a variable through the GOTO block, which then is read using the FROM block.

6.1.2 Testing the resulting system

We have seen in Section 4.5.1 that the open-loop controller on land works, and we have seen in Section 5.5.2 that the autopilot works. What is new for this section is the changing initial condition for the integrators, so this is what should be tested here. To do this we try to maneuver the vessel towards an imagined shore, where we do a u-turn on land and return to the water with the opposite heading to when the vessel made landfall. If the initial conditions do what they should, then the entry back into water should be a simple matter.

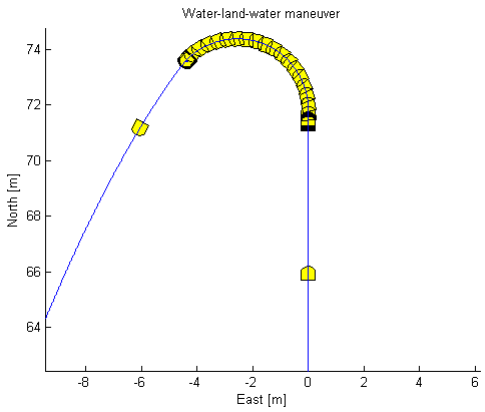

Figure 6.1: Combined model maneuver

As we see in this figure, this seems to be the case. The autopilot gets the new heading from the land-based model and, since the joystick point that way, keep moving in that direction seemingly bumpless.

A bug in the design has emerged when creating the plots showing the performance of the system. The system is supposed to recognize which buttons the operator presses on the joystick and only begin using the land model for one, or a combination of two, buttons. It does however seem that this is not the case, and that the system sets all positions and velocities to zero when any other button is pressed. This was discovered too late for any meaningful debugging to be done.

Chapter 7

Hardware-in-the-loop testing and model validation

The developed models for land and water is separately implemented in LabView in preparation for future hardware-in-the-loop testing.

7.1 LabView implementation

LabView, short for Laboratory Virtual Instrumentation Engineering Workbench, is a visual programming language developed by National Instruments, which is meant to automate the use of processing and measurement equipment in a laboratory. It is designed to effectively manage input and output signals, but when it comes using these signals in calculations programs like Simulink is better suited. This is why National Instruments have developed a compiler that translates Simulink diagrams into code understandable to LabView. However, this compiler is only made for Windows XP and the 2009 version of Simulink, which makes it quite impractical as you need a designated computer with this setup in order to make it work.

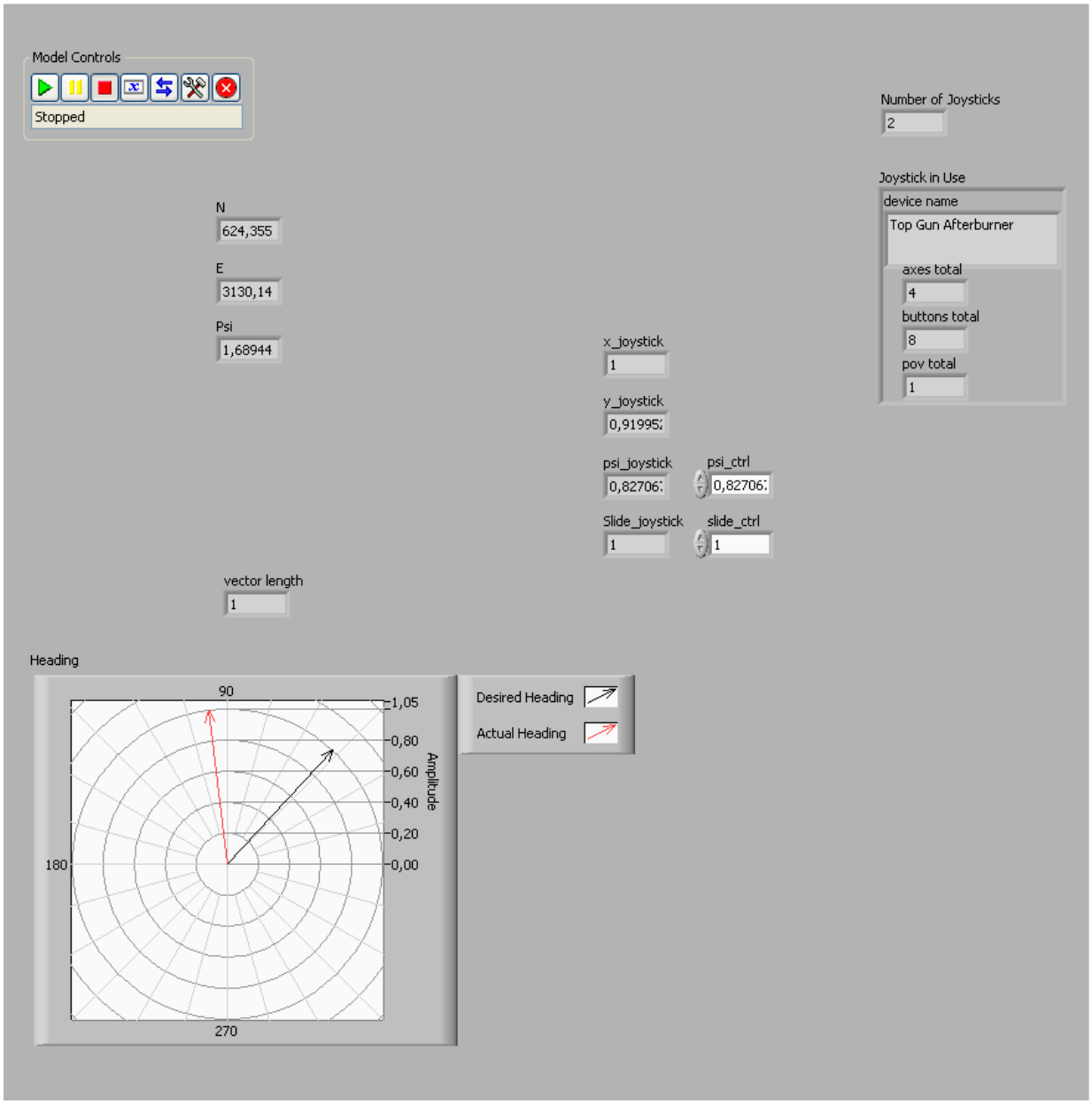

Figure 7.1: Front panel of LabView interface

Since LabView is meant to be an input and output manager, it comes with a variety of ways to visualise these inputs and outputs. In Figure 7.1 we see the setup used testing the developed model. The compass shows actual and desired heading while the numerical indicators show the position of the vessel and the position of the joystick at any given time. in the top right corner is information about the joystick currently connected.

7.2 Hardware-in-the-loop

Hardware-in-the-loop (HIL) testing is a method used in various industries to test its product in a simulation of the real world, and hopefully detect and remove faults, before launching it.

7.2.1 Background

HIL is a method of testing that has risen with the increasing power of computers, and makes it possible to get more and more accurate replications of real world conditions. In the aerospace and automobile industry this has been done for a while, but the marine industry is quite conservative and has only recently started exploring the possibilities in HIL. When a new ship launched, all the systems have been individually tested for bugs and faults. The vessel as an entity is tested during sea trials and here bugs and faults for the interconnected systems are discovered. However, sea trials are expensive. What HIL testing introduces is the capability of testing the interconnected system while the vessel is still in dry dock being built. This does not remove the need for sea trials, but with good HIL testing the chances of finding faults during these trials are reduced and the vessel will therefore be deemed finished sooner.

HIL testing works by uploading the mathematical model of the real world process onto a real-time platform and to connect this to the electronic control unit designed to control that process. The term real-time is used to distinguish between real world time and computer simulation time. Because the simulation time on a computer is depending, among other things, on the frequency of the processing unit, a process run over minutes in simulated time may be done in seconds in real world time. Providing real-time constraints then lessens the need for quick processing units and also does a much better jobs at identifying faults whose source lies in sample rates and timing.

7.2.2 CompactRIO

The real-time platform used in MCLab is the CompactRIO (Reconfigurable I/O). This is a device developed by the same company that makes the LabView program, and is therefore compatible with LabView models. Whereas in HIL testing, the RIO is used to hold the model of the real world process and a connected computer provides the control algorithm to be tested, the uses can be reversed. If the controller is uploaded on the RIO one can put it physically in the model vessel and use the controller output to control the vessel, and tune the controller while testing. For this thesis, both the model of the vessel and the controller were uploaded in order to see better identify the real-time response of the developed system.

7.2.3 Testing the RIO

The task here was to transfer the Simulink model to the CompactRIO and run the LabView script through that, in order to test the model in real time and to learn how to use the CompactRIO. This took some time to achieve as there were problems with the CompactRIO software that communicated with LabView. Because this took quite some time to fix, there ended up being no time to do anything else than to see that the model worked. No proof that the test took place can be given, other than a description of the results which were quite strange. A change in desired heading given by the joystick did result in convergence, but the rate was very slow. Since all tests prior to this had been done on simulated time, this had not been noticed before now. It is not known what causes this. The same thing was seen in both the models.

7.3 Validation

A mathematical model of a vessel is made up of the rigid-body dynamics, the hydrodynamics and the thrust allocation of the vessel. When validating such a model one runs the real vessel through a set of movements and takes measurements of the resulting movements one wishes to look at. The mathematical model is then put through the exact same input, and the calculated movements are then compared to the ones from the real vessel.

7.3.1 Goals

The experiments done in MCLab were to detect bollard-pull in surge and sway, and the yaw moment generated by these forces. Surge damping was also tested. The goal when validating the resulting model must therefore be to see if the produced thrusts and damping equals the ones determinated in Chapter 3.

7.3.2 Result

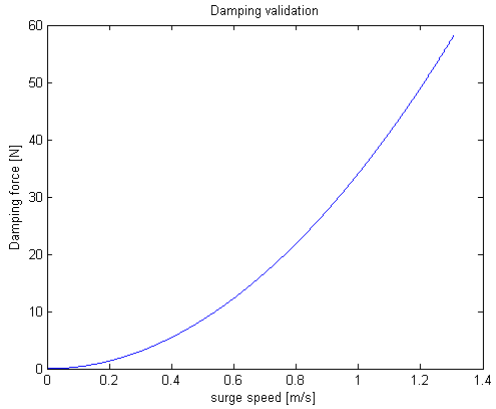

Figure 7.2: Validation of surge damping

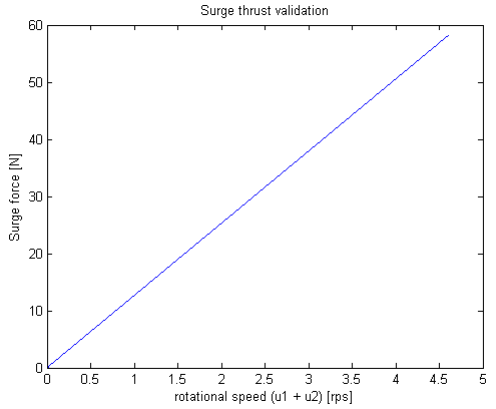

Figure 7.3: Validation of produced surge thrust

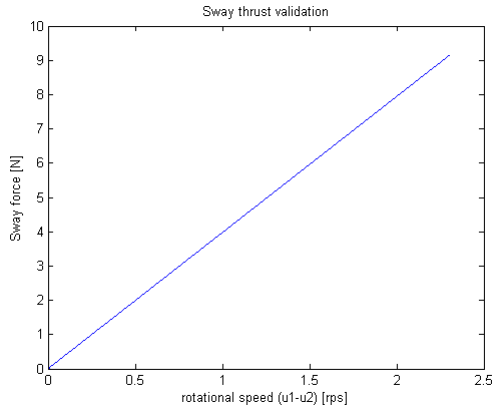

Figure 7.4: Validation of produced sway thrust

Comparing Figures 7.2, 7.3 and 7.4 to Figures 3.6, 3.8 and 3.10 respectively shows that they fit almost perfectly.

7.3.3 Discussion

The thrust is calculated directly from the experimental results, so it is no surprise that they fit. When comparing the surge damping, we see a slight difference. This is because the linear component of the damping was removed since it was given as a negative value. It was argued that it was so small that it would make very little impact if removed all together which proved to be correct.

No measurement has been done of position as a function of screw speed. There is therefore no possibility of validating the model as accurately as is desirable. For accurate mathematical model, a wireless data gathering scheme must be implemented as the current setup with wires sticking out of the back-end of the model does not allow for free movement.

Chapter 8

Concluding remarks

8.1 Conclusion

The task in this thesis was to develop a mathematical model of the AMV OSF vessel model, and design a control system for both land and water operations. The mathematical model was determined with some of its parameters found through testing the vessel model in the MCLab. The remaining parameters were given an assumed value. The developed model managed to reproduce the results from the experiment very accurately. When the model was finished, the straight-line stability of the model was analyzed and it was concluded that the mathematical model was unstable.

Because of the amphibious nature of the vessel, two control modes were needed. One to use on land, and one on water. It was decided that the land model should be controlled through an open-loop, where the body-fixed velocity was set directly by the joystick used as input. It was then argued that the water model should be an autopilot with closed-loop heading control and open-loop surge-speed control, where the joystick provides desired heading and surge speed. Two different autopilots were made to pick the one with best performance, but both the PID and the linear backstepping controller ended up producing almost identical results.

These controllers seem work fine when when tested individually, as seen from the simulation results, so they were then combined to make one model intended to be as close to the real vessel model as possible. In the combined model, the land and water mode needed to share their position, heading and velocities so that when the mode was switched the integrators knew where to start from. According to tests, the combined model does what is expected, providing seemingly bumpless transition between the two modes, land and water. The joystick is to be used to provide input to the different controllers and to tell the model which medium, land or water, the vessel operates on.

A method of turning the vessel up against incoming current and still keep heading control were devised, and the results shows the heading difference quite clearly, while the course is kept as desired.

At the end, transferring the model to the a CompactRIO was achieved, although with some unexplained responses from the model.

8.2 Further Work

In order to develop an accurate mathematical model for the full-scale vehicle, more accurate parameters will have to be identified. Without this, any tests done will be suitable only for proving concepts and testing ideas. Therefore, the first objective for any further work should be to determine these through model testing. Since the development of the full-scale vessel is an ongoing process, it should be considered to create a model vessel that has the same dimensions as the current full-scale vessel.

Here, the moment of inertia, I_z, is calculated with the assumption that the mass of the vehicle is evenly distributed. This is not viable for the full scale I_z because of the big weight presence of equipment like engine and fuel-tank

From observing the model's performance in MCLab and from talking about the full-scale prototype's performance during its first test on water it is suspected that the assumption of small roll angles in normal operation is invalid. The screws rotate quite fast and generate a momentum. When the screws rotate at the same speed these moments erase each other. But when the speeds are different, the resulting moment may cause a large roll angle. This needs to be verified and, if it proves to be the case, implemented in the model.

If the model is deemed accurate enough, the next step would be to equip an OSF model with a CompactRIO and upload a controller into this. Since the controller developed in this thesis will only give the screws desired rotational speed, measurements of the elector motors voltage as a function of this speed must be gathered in order to test any new controller.

Bibliography

Berg, T. E. (2009), *Ship Manoeuvering*, Marinteknisk Senter. Lecture note for TMR4220.

Engelbreth, K. I. (2009), 'Model test of an archimedes' screw applied as a marine propulsive unit'. Project in the subject AT-327 Arctic Offshore Engineering at the University Centre at Svalbard.

Faltinsen, O. (1990), *Sea loads on ships and offshore structures*, Cambridge University Press.

Fossen, T. I. (2010), *Guidance and control of marine craft*. Draft copy for proofreading.

Fossen, T. I. (2011), *Handbook of Marine Craft Hydrodynamics and Motion Control*, John Wiley & Sons, Ltd.

Greco, M. (2010), 'Lecture notes week 36'. Lecture note from lectures in TMR4215.

Irgens, F. (1979), *Fasthetslære*, 6. edn, Tapir Forlag. Norwegian.

Nilsen, L. M. F. (2010), 'Modeling and control of the amv oil spill fighter'. Preliminary work to this thesis.

Rorres, C. (2000), 'The turn of the screw: Optimal design of an archimedes screw'.

Sørensen, A. J. (2006), *Marine Cybernetics: Modelling and Control*, Department of marine technology NTNU.